Investigation into the Valence Electronic Structure of Norbornene Using Electron Momentum Spectroscopy, Green's Function, and Density Functional Theories

S. Knippenberg,[†] K. L. Nixon,[‡] H. Mackenzie-Ross,[‡] M. J. Brunger,*[,‡] F. Wang,[||] M. S. Deleuze,*[,†] J.-P. François,[†] and D. A. Winkler[⊥]

Group of Theoretical Chemistry, Department SBG, Hasselt University, Agoralaan, Gebouw D, B-3590 Diepenbeek, Belgium, School of Chemistry, Physics and Earth Sciences, Flinders University, GPO Box 2100, Adelaide SA 5001, Australia, Centre for Molecular Simulation, Swinburne University of Technology, PO Box 218, Hawthorn, Vic 3122, Australia, and CSIRO Molecular Science, Private Bag 10, Clayton South MDC, Vic 3169, Australia, and School of Chemistry, Monash University, Clayton, Vic 3168, Australia

Received: May 10, 2005; In Final Form: July 7, 2005

Results of a study of the valence electronic structure of norbornene (C_7H_{10}), up to binding energies of 30 eV, are reported. Experimental electron momentum spectroscopy (EMS) and theoretical Green's function and density functional theory approaches were utilized in this investigation. A stringent comparison between the electron momentum spectroscopy and theoretical orbital momentum distributions found that, among the tested models, the combination of the Becke−Perdew functional and a polarized valence basis set of triple-ζ quality provides the best representation of the electron momentum distributions for all 19 valence orbitals of norbornene. This experimentally validated model was then used to extract other molecular properties of norbornene (geometry, infrared spectrum). When these calculated properties are compared to corresponding results from independent measurements, reasonable agreement is typically found. Due to the improved energy resolution, EMS is now at a stage to very finely image the effective topology of molecular orbitals at varying distances from the molecular center, and the way the individual atomic components interact with each other, often in excellent agreement with theory. This will be demonstrated here. Green's Function calculations employing the third-order algebraic diagrammatic construction scheme indicate that the orbital picture of ionization breaks down at binding energies larger than about 22 eV. Despite this complication, they enable insights within 0.2 eV accuracy into the available ultraviolet emission and newly presented (e,2e) ionization spectra. Finally, limitations inherent to calculations of momentum distributions based on Kohn−Sham orbitals and employing the vertical depiction of ionization processes are emphasized, in a formal discussion of EMS cross sections employing Dyson orbitals.

1. Introduction

The bicyclo [2.2.1] seven-membered hydrocarbon cages, of which bicyclo [2.2.1]-2-heptene or norbornene (C_7H_{10}) is a member, have frequently been used to fix geometric variables in structure/reactivity studies and in the probing of the relationship between spectroscopic properties and structure.[1] The framework (see Figure 1) consists of a six-membered ring held in a "boat" conformation that serves as a model system for the transition state for "chair-chair" interconversion in the chemically important six membered ring. The additional bridgehead ("7") group subtends a less-than-ideal angle for a saturated linkage and is thus expected to exhibit (and act as a vehicle for studying) strain effects. The electronic structure of the norbornene (NBN) ring system also predisposes it toward rapid reaction on the exo face of the double bond.[2,3] Though several theoretical explanations exist (see, for example, refs 4 and 5), the origin of the exceptional reactivity has eluded unequivocal physical detection. More recently,[6] femtosecond-resolved spectroscopic detection of intermediates in a simple retro Diels−Alder[7] reaction has created considerable excitement. The thermal unimolecular dissociation of NBN into ethylene and cyclopentadiene is a classic illustration of the retro Diels−Alder reaction,[6] the mechanisms of which are still somewhat controversial.[8]

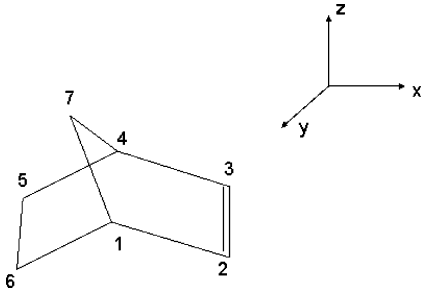

Figure 1. Structural representation of norbornene and the atom numbering.

In all of the above examples of the chemical importance of NBN, whether it be for an unambiguous determination of its structure or a mechanistic description of its role in various reactions, quantum chemical calculations play a major role in assisting our understanding.[9] However, the results of these calculations are often very sensitive to the type of theory employed (including the basis set used),[6] so that a technique

* Corresponding authors. E-mail: M.J.B., Michael.Brunger@flinders.edu.au; M.S.D., Michael.Deleuze@uhasselt.be.
[†] Hasselt University.
[‡] Flinders University.
[||] Swinburne University of Technology.
[⊥] Monash University.

10.1021/jp058158z CCC: $30.25
Published on Web 09/02/2005

that validates a priori quantum chemical models is potentially very useful. The unique orbital imaging capability of electron momentum spectroscopy (EMS)[10,11] can in principle fulfill just such a role and here we report on its application to NBN. Specifically, we use EMS to determine which of our employed density functional theory (DFT) exchange correlation functionals and basis sets best describe the experimental momentum distributions. This optimum basis and exchange correlation functional is then used to derive the molecular geometry of norbornene. That data are next compared with independent experimentally determined values, and those from other MO calculations, to determine how well the optimum model was able to reproduce norbornene's molecular geometry.

While conducting our study, it became quite clear that existing investigations into the outer- and inner-valence electronic structure of norbornene are rather scarce. Previous photoelectron spectroscopy (PES) studies include the He (I) measurements from Bischof et al.,[12] Demeo and Yencha[13] and Wen et al.[14] and the He (II) measurement from Bieri et al.[15] Theoretical interpretation of these spectra has been even more limited with only the modified intermediate neglect of differential overlap, version 2 (MINDO/2) result from Bodor et al.[16] being available in the literature. Hence the present Hartree−Fock (HF), density functional theory (DFT) and one-particle Green's function (1p-GF) calculations significantly expand the available theoretical knowledge of the electronic structure of norbornene. In addition, we believe that the present EMS measurements are the first to be made on this molecule, thus further expanding our understanding of its electronic structure through our original momentum space images of its molecular orbitals (MOs).

In the next section of this paper we discuss briefly our EMS measurements, including our ionization spectra. Details of our HF, DFT, and 1p-GF calculations, and some of the electronic structure information we can extract from them by investigating the EMS cross sections and the valence ionization spectra, are presented in sections 3 and 4, respectively. In section 5 we compare and discuss the experimental and theoretical momentum distributions associated to all bands in the EMS ionization spectra. In section 6 the molecular geometry derived from our optimum basis set and exchange correlation functional is detailed, and in section 7 some of the conclusions drawn from the current study are presented.

2. Experimental Details and Preliminary Analysis

A sample of norbornene was purchased from the Aldrich Chemical Co. As the quoted purity was greater than 99.99%, this sample was used in our measurements without further purification. Note, however, that as EMS is highly sensitive to the presence of any impurities, our NBN sample was degassed in situ by repeated freeze−pump−thaw cycles of its storage vessel before being introduced into the interaction region.

All 19 occupied MOs of the complete valence region of NBN, namely the 12a′, 7a ″, 6a ″, 11a′, 10a′, 9a′, 5a″, 4a″, 8a′, 7a′, 6a′, 5a′, 3a″, 4a′, 2a″, 3a′, 1a″, 2a′, and 1a′ MOs, were then investigated in several experimental runs using the Flinders symmetric noncoplanar EMS spectrometer.[10] Details of this coincidence spectrometer and the method of taking the data can be found in Brunger and Adcock[11] and Weigold and McCarthy,[10] so we do not repeat them again here.

The high-purity NBN sample was admitted into the target chamber through a capillary tube, the flow rate being controlled by a variable leak valve. Possible clustering due to supersonic expansion was avoided by maintaining a low NBN driving pressure throughout data collection. The collision region was differentially pumped by a 700 l s^{-1} diffusion pump. Apertures and slits were cut in the collision chamber for the incident electron beam and the scattered and ejected electrons. Our (e,2e) monochromator[11] typically produces incident electron beam currents of the order of 30 μA into the interaction region, with the overall coincident energy resolution of the present measurements being ∼0.6 eV full-width-at-half-maximum (FWHM). Note that the coincident energy resolution was determined from measurements of the binding-energy (ϵ_f) spectrum of helium, whose profile was found to be well represented by a Gaussian function. However, due to the natural and vibrational line widths (Franck−Condon widths) of the various electronic transitions and a quite strong dispersion of the ionization intensity into many-electron processes at the bottom of the carbon-2s region, the fitted resolutions of the spectral peaks for NBN varied from ∼0.90 to 2.45 eV (FWHM). It is precisely this limitation that forces us to combine our measured 6a″, 11a′, 10a′, 9a′, and 5a″ orbital momentum distributions (MDs), 4a″ and 8a′ orbital MDs, 5a′ and 3a″ orbital MDs, 4a′ and 2a″ orbital MDs, and 3a′, 1a″, and 2a′ orbital momentum distributions, respectively. Although there is no doubt one loses some physical information in combining these MDs, to not do so would have raised serious question as to the uniqueness of the MDs derived in the fits to our binding energy spectra (see below). The angular resolution, which determines the momentum resolution (see eq 1), was typically 1.2° (FWHM) as determined from the electron optics and apertures and from a consideration of the argon 3p angular correlation.

In the present study, noncoplanar symmetric kinematics was employed. That is, the outgoing electron energies E_A and E_B were equal (=750 eV) and the scattered (A) and ejected (B) electrons made equal polar angles, $\theta = 45°$, with respect to the direction of the incident electrons. The total energy (E), $E = E_0 - \epsilon_f = E_A + E_B$, was 1500 eV. The beam energy was E_0. The binding-energy range of interest (ϵ_f = 6−30 eV) was stepped through sequentially at each of a chosen set of azimuthal angles ϕ using a binning mode,[17] through the entire range of azimuthal angles ($\phi = 0° - 30°$). Scanning through a range of ϕ is equivalent to sampling different target electron momenta $\mathbf{p}$ as[10]

$$p = \left[(2p_A \cos\theta - p_0)^2 + 4p^2{}_A \sin^2\theta \sin^2\left(\frac{\phi}{2}\right)\right]^{1/2} \quad (1)$$

For zero binding-energy ($\epsilon_f = 0$ eV), $\phi = 0°$ corresponds to $p = 0$ au. For the present binding energies, angular resolution and kinematics, $\phi = 0°$ corresponds to $p \approx 0.03$ au. Note that 1 au $\equiv 1a_0^{-1}$, where a_0 = Bohr radius (0.5292 Å).

Ionization spectra of norbornene measured at representative angles ϕ in the region 6−30 eV and at E = 1500 eV are displayed in Figure 2. The solid curve in each panel represents the envelope of the 12 fitted Gaussians (various dashed curves) whose positions below $\epsilon_f \sim 23$ eV are taken from the available PES data.[12−15] A summary of the available orbital binding energies from PES data,[12,15] the present EMS binding energies, and our tentative orbital assignments are given in Table 1a. The fact that we used only 12 Gaussians to analyze spectra containing 19 valence MOs simply reflects our earlier point that our energy resolution was insufficient to uniquely deconvolve all the orbitals, so that some were combined (summed). Notwithstanding this, it is clear from Figure 2 that the fits to the measured binding-energy spectra are excellent. The least-squares-fit deconvolution technique used in the analysis of these

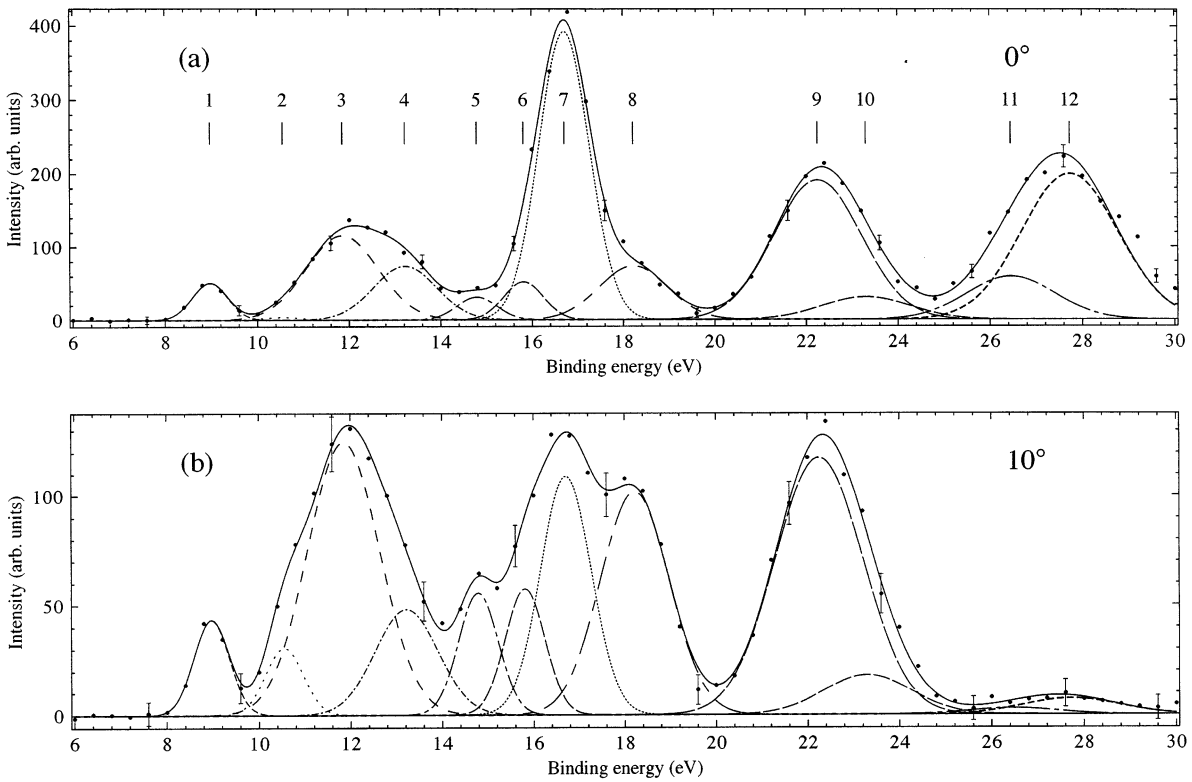

Figure 2. Typical binding-energy spectra from our 1500 eV noncoplanar symmetric EMS investigation into norbornene. The curves show the fits to the spectra at (a) $\phi = 0°$ ($p \approx 0.03$ au) and (b) $\phi = 10°$ ($p \approx 0.92$ au) using the known energy resolution. Note that indicative error bars are shown on this figure, and that the peak positions of the Gaussians used in the fit (see also Table 1a) are indicated.

spectra is based on the work of Bevington and Robinson,[18] to whom readers are referred for more detail. Above $\epsilon_f \sim 23$ eV there are no PES data available to guide us in our fitting of the binding-energy spectra. Under these circumstances the positions and widths of the Gaussian peaks, and the number of Gaussians, used in the spectral deconvolution were simply determined by their utility in best fitting the observed data for all ϕ. The fact that the inner valence 3a′, 1a″, 2a′, and 1a′ orbitals need 4 very broad Gaussians to incorporate the measured coincidence intensity into the fit, is undoubtedly indicative of a severe dispersion of ionization intensity over many satellite states. This observation led us to undertake thorough one-particle Green's function (1p-GF) calculations of the valence one-electron and shake-up ionization spectrum of norbornene (see section 4).

The EMS ionization spectra of Figure 2 clearly reflect the respective symmetries[10] of the valence orbitals of norbornene. For instance the next-highest-occupied-molecular-orbital (NHOMO, peak 2 of Figure 2) exhibits significantly more intensity at $\phi = 10°$ compared to that at $\phi = 0°$. This is consistent with the "p-type" symmetry of this orbital. On the other hand the unresolved 5a′ and 3a″ orbitals (peak 7) have a much greater intensity at $\phi = 0°$ compared to that found at $\phi = 10°$ (almost 4:1), which corroborates the dominance of an "s-type" symmetry. On the basis of the symmetry indicated by the EMS binding-energy spectra and the results of our calculations in Table 1b (see section 3 for more details) tentative orbital assignments were made and are given in both Tables 1a and 1b. In general these orbital assignments are consistent with those found from our 1p-GF calculations (see Table 2). The angular dependence of the EMS cross sections indicate that peaks 11 and 12 have similar "s-type" MDs, so that both peaks at first glance could be ascribed to originating from the 1a′ orbital. Our 1p-GF calculations, however, do not find any ionization lines with a pole (spectroscopic) strength larger than 0.005 at binding energies greater than 26 eV. This latter result is due to the extreme shake-up fragmentation in this region of the binding-energy spectrum arising because of the very low symmetry of the norbornene compound, enabling many configuration interactions in the cation. Without theoretical support from our 1p-GF calculation, our assignment of peaks 11 and 12 in Figure 2 must therefore remain tentative at this time.

3. Theoretical Analysis of EMS Cross Sections

The very first assumption used to analyze the measured cross sections for high-momentum transfer (e,2e) collisions is the so-called binary-encounter approximation (also referred to as the "Born", "sudden" or, more specifically in the present framework, "weak-coupling" approximation[10,19]). It consists of simply equating the wave function of the neutral N-electron system after ionization to an (antisymmetrized) product of the $N - 1$ cationic wave function (Ψ_f^{N-1}) and of a one-electron scattering wave function ($\mathbf{q}$) for the outgoing electron. Invoking the Born−Oppenheimer approximation for both the neutral and ion wave functions, the EMS differential cross sections σ, for randomly oriented molecules and unresolved rotational and vibrational states, is given by[10]

$$\sigma = K \int \mathrm{d}\Omega \, |\langle \mathbf{q}\Psi_f^{N-1} | \Psi_0^N \rangle|^2 \qquad (2)$$

where K is a kinematical factor that is essentially constant in the present experimental arrangement. Along with the Born approximation, a vertical depiction for the ionization process is most commonly assumed (i.e., geometrical relaxation and-

TABLE 1

a. Experimental Electronic Structure of Norbornene[a,b]

orbital no.	classification present	ϵ_f (eV) experimental: PES[12,15]	ϵ_f (eV) experimental: present EMS
1	12a′	8.97	8.97
2	7a″	10.55	10.55
3	6a″	11.85	11.85
4	11a′		
5	10a′		
6	9a′		
7	5a″		
8	4a″	13.22	13.22
9	8a′		
10	7a′	14.79	14.79
11	6a′	15.81	15.81
12	5a′	16.71	16.71
13	3a″		
14	4a′	18.22	18.22
15	2a″		
16	3a′	22.25	22.25, 23.30
17	1a″		
18	2a′		
19	1a′		26.45, 27.73

b. Theoretical Electronic Structure Calculations for Norbornene[b]

orbital no.	classification present	ϵ_f (eV): present SCF RHF/TZVP	present DFT LSD/TZVP	present DFT BLYP/TZVP	present DFT BP/TZVP
1	12a′	9.21	5.83	5.51	5.75
2	7a″	11.70	7.20	7.06	7.25
3	6a″	12.30	7.96	7.62	7.87
4	11a′	12.65	8.10	7.83	8.06
5	10a′	13.19	8.22	8.06	8.25
6	9a′	13.20	8.39	8.16	8.38
7	5a″	13.40	8.43	8.23	8.42
8	4a″	14.44	9.25	9.01	9.23
9	8a′	15.06	9.56	9.34	9.55
10	7a′	16.38	10.78	10.44	10.70
11	6a′	17.52	11.70	11.27	11.57
12	5a′	18.94	12.38	12.24	12.49
13	3a″	19.14	12.71	12.31	12.60
14	4a′	20.84	13.55	13.39	13.64
15	2a″	21.67	14.08	13.97	14.22
16	3a′	25.71	17.00	16.72	17.05
17	1a″	26.38	17.62	17.25	17.61
18	2a′	27.43	18.22	17.90	18.25
19	1a′	32.04	22.06	21.35	21.84

[a] Our tentative classifications for the valence orbitals are also given in this table. [b] All binding energies (ϵ_f) are given in eV.

nuclear dynamical effects are neglected). In the above equation, Ψ_0^N is the target [N electron] ground state. Invoking further the plane wave impulse approximation (PWIA),[19] and neglecting therefore the residual interactions between the outgoing electrons and the remaining cation, **q** is reduced to a plane wave. $\int d\Omega$ denotes the integral required for averaging the computed (e,2e) cross sections over all gas-phase molecular orientations (spherical averaging). The average over the initial vibrational state is well approximated by evaluating orbitals at the equilibrium geometry of the molecule. Final rotational and vibrational states are eliminated by closure.[10]

The momentum space target-ion overlap $\langle \boldsymbol{q}\Psi_f^{N-1}|\Psi_0^N\rangle$ can be evaluated using configuration interaction (CI) descriptions of the many-body wave functions.[20] Within an exact theoretical framework, in straightforward analogy with the scheme developed by Deleuze et al.[21] to compute photoionization intensities, the transition amplitude of eq 2 can be recast as a structure factor derived as a Fourier Transform of a Dyson spin−orbital for the ionization channel (f) under consideration,

$$\sigma_f = K\int d\Omega\ |g_f(\omega,\vec{p})|^2 \qquad (3)$$

where the corresponding Dyson spin−orbital $g_f(\mathbf{x})$ is defined as the partial overlap between the neutral ground state and final cationic state:

$$g_f(\mathbf{x}) = \sqrt{N}\int \Psi_f^{N-1}(\mathbf{x}_1,\mathbf{x}_2,...,\mathbf{x}_{N-1})\,\Psi_0^N(\mathbf{x}_1,\mathbf{x}_2,...,\mathbf{x}_{N-1};\mathbf{x})\,d\mathbf{x}_1\,d\mathbf{x}_2\,...\,d\mathbf{x}_{N-1} \qquad (4)$$

with N being the number of electrons. In eqs 3 and 4, ω (=α or β) and $\mathbf{x}_i = (\omega_i,\vec{r}_i)$ represent electron spin and electron spin-space coordinates, respectively.

Dropping spin for simplicity, and expanding the Dyson orbitals in a canonical MO basis, the target-ion overlap of eq 2 can be replaced by a structure factor derived as the Fourier

TABLE 2: Present ADC(3) and OVGF Calculation Results for the Electronic Structure of Norbornene[a]

			ADC(3)/ cc-pVDZ(I)		OVGF/ cc-pVDZ(I)		OVGF/ aug-cc-pVDZ(I)		OVGF/ cc-pVTZ(I)		OVGF/ cc-pVDZ(II)		OVGF/ cc-pVDZ(III)	
symbol	label	HF/cc-pVDZ(I) ϵ_f (eV)	ϵ_f (eV)	Γ_f	ϵ_f (eV)	Γ_f	ϵ_f (eV)	Γ_f	ϵ_f (eV)	Γ_f	ϵ_f (eV)	Γ_f	ϵ_f (eV)	Γ_f
s	12a′	9.117	8.975	0.899	8.855	0.907	8.972	0.905	8.909	0.904	8.874	0.907	8.749	0.906
r	7a″	11.682	10.838	0.905	10.717	0.910	10.832	0.908	10.796	0.907	10.722	0.910	10.746	0.910
q	6a″	12.215	11.388	0.901	11.239	0.907	11.353	0.905	11.281	0.904	11.260	0.907	11.232	0.906
p	11a′	12.604	11.749	0.903	11.628	0.908	11.739	0.906	11.685	0.905	11.650	0.908	11.624	0.907
n	10a′	13.102	12.166	0.902	12.042	0.909	12.152	0.907	12.102	0.906	12.061	0.909	11.981	0.909
m	9a′	13.148	12.101	0.899	11.972	0.904	12.102	0.902	12.044	0.902	11.987	0.904	11.912	0.904
l	5a″	13.339	12.322	0.905	12.232	0.910	12.340	0.908	12.308	0.908	12.237	0.911	12.225	0.910
k	4a″	14.376	13.280	0.895	13.186	0.905	13.298	0.903	13.271	0.902	13.197	0.906	13.183	0.905
j	8a′	14.910	13.684	0.895	13.560	0.903	13.688	0.901	13.638	0.900	13.588	0.903	13.453	0.903
i	7a′	16.282	15.003	0.780	15.004	0.899	15.114	0.896	15.074	0.896	15.039	0.899	14.952	0.898
			15.295 (i)[b]	0.074										
h	6a′	17.390	15.945	0.503	15.829	0.894	15.890	0.891	15.893	0.890	15.857	0.894	15.769	0.893
			16.151 (ii)	0.416										
			19.478	0.011										
g	5a′	18.778	17.160	0.826	16.995	0.881	17.071	0.878	17.068	0.878	17.043	0.882	16.916	0.881
			17.954 (iii)	0.055										
f	3a″	19.097	16.765 (iv)	0.044	17.147	0.877	17.210	0.874	17.233	0.874	17.157	0.878	17.108	0.876
			17.083	0.151										
			17.268	0.647										
e	4a′	20.757	18.494	0.604	18.531	0.864			18.588	0.860	18.559	0.865	18.438	0.863
			19.122 (v)	0.223										
			20.785	0.009										
d	2a″	21.633	18.669 (vi)	0.048	19.621	0.858			19.320	0.853	19.278	0.858	19.183	0.854
			19.215	0.657										
			19.781	0.068										
			19.945	0.010										
			20.201	0.008										
			20.288	0.024										
			20.342	0.025										
			21.703	0.010										
c	3a′	25.627	20.964	0.007	22.544	0.811[c]					22.581	0.812[c]		
			21.271	0.009										
			21.631	0.006										
			21.675	0.007										
			21.866	0.015										
			22.010	0.051										
			22.090	0.021										
			22.164	0.122										
			22.176	0.008										
			22.278	0.006										
			22.294	0.060										
			22.319	0.151										
			22.407	0.040										
			22.450	0.009										
			22.484	0.009										
			22.675	0.010										
			22.764	0.059										
			22.834	0.030										
			22.856	0.040										
			22.864	0.124										
			22.931	0.059										
			22.977	0.015										
			23.106	0.007										
			23.200	0.009										
b	1a″	26.331	21.548	0.009										
			22.008	0.009										
			22.194	0.006										
			22.237	0.015										
			22.307	0.020										
			22.515	0.029										
			22.541	0.010										
			22.611	0.016										
			22.651	0.006										
			22.756	0.014										
			22.820	0.017										
			22.846	0.008										
			22.895	0.011										
			22.903	0.029										
			23.011	0.225										
			23.039	0.047										
			23.119	0.054										

TABLE 2 (Continued)

			ADC(3)/ cc-pVDZ(I)		OVGF/ cc-pVDZ(I)		OVGF/ aug-cc-pVDZ(I)		OVGF/ cc-pVTZ(I)		OVGF/ cc-pVDZ(II)		OVGF/ cc-pVDZ(III)	
symbol	label	HF/cc-pVDZ(I) ϵ_f (eV)	ϵ_f (eV)	Γ_f	ϵ_f (eV)	Γ_f	ϵ_f (eV)	Γ_f	ϵ_f (eV)	Γ_f	ϵ_f (eV)	Γ_f	ϵ_f (eV)	Γ_f
			23.155	0.007										
			23.180	0.057										
			23.224	0.030										
			23.292	0.026										
			23.309	0.016										
			23.381	0.016										
			23.401	0.016										
			23.416	0.008										
			23.476	0.013										
			23.568	0.009										
a	2a′	27.311	23.168	0.006										
			23.261	0.010										
			23.372	0.027										
			23.420	0.014										
			23.493	0.010										
			23.555	0.011										
			23.581	0.019										
			23.609	0.010										
			23.627	0.009										
			23.658	0.007										
			23.685	0.026										
			23.694	0.064										
			23.732	0.060										
			23.792	0.007										
			23.834	0.010										
			23.901	0.031										
			23.968	0.010										
			24.000	0.084										
			24.008	0.017										
			24.046	0.027										
			24.086	0.008										
			24.255	0.006										
			24.315	0.006										

Dominant Electronic Configurations:

i	$12a'^{-1}$	$7a''^{-1}$	$8a''^{+1}$	$[(HOMO)^{-1}$	$(HOMO\text{-}1)^{-1}$	$(LUMO)^{+1}]$	
ii	$12a'^{-1}$	$6a''^{-1}$	$8a''^{+1}$	$[(HOMO)^{-1}$	$(HOMO\text{-}2)^{-1}$	$(LUMO)^{+1}]$	
iii	$12a'^{-1}$	$4a''^{-1}$	$8a''^{+1}$	$[(HOMO)^{-1}$	$(HOMO\text{-}7)^{-1}$	$(LUMO)^{+1}]$	
iv	$12a'^{-1}$	$9a'^{-1}$	$8a''^{+1}$	&	$12a'^{-1}$	$10a'^{-1}$	$8a''^{+1}$
	$[(HOMO)^{-1}$	$(HOMO-5)^{-1}$	$(LUMO)^{+1}]$	&	$[(HOMO)^{-1}$	$(HOMO\text{-}4)^{-1}$	$(LUMO)^{+1}]$
v	$12a'^{-1}$	$7a''^{-1}$	$8a''^{+1}$	$[(HOMO)^{-1}$	$(HOMO\text{-}1)^{-1}$	$(LUMO)^{+1}]$	
vi	$12a'^{-1}$	$8a'^{-1}$	$8a''^{+1}$	$[(HOMO)^{-1}$	$(HOMO\text{-}8)^{-1}$	$(LUMO)^{+1}]$	

[a] The binding energies (ϵ_f) are given in eV, along with the OVGF and ADC(3) spectroscopic factors (Γ_f). (I) using B3LYP/TZVP geometry. (II) using B3LYP/cc-pVTZ geometry and (III) using MP2/aug-cc-pVDZ geometry. [b] Dominant electronic configurations given at bottom of table. [c] Breakdown of the MO picture of ionization (*J. Chem. Phys.* **2002**, *116*, 7012).

transform of the relevant Hartree−Fock or Kohn−Sham ground state, multiplied by a spectroscopic amplitude (or strength Γ_f) defined as the norm of the Dyson orbital pertaining to the ionization channel *f*:

$$\sigma_f = K \sum_j S_j^{(f)} \int \mathrm{d}\Omega \, |\phi_j(\vec{p})|^2 \tag{5}$$

$$\approx K \, \Gamma_f \int \mathrm{d}\Omega \, |\phi_j(\vec{p})|^2 \tag{6}$$

with ϕ_j the ionized orbital. Note that one further approximation has been taken with eq 6, which amounts to neglecting the consequences of electronic relaxation on orbitals (for one-electron ionization processes, the fraction of intensity that is lost into secondary shake-up processes is equal to $1 - \Gamma_f$). Despite this neglect, the basis of the orbital imaging capability of EMS is immediately apparent from eqs 5 and 6.

In an exact many-electron framework, the spectroscopic strength of state *f* is obtained (see further) as

$$\Gamma_f = \sum_j S_j^{(f)} \tag{7}$$

with $S_j^{(f)}$ the square of the Feynman−Dyson transition amplitudes for ion state *f* and orbital *j*:

$$S_j^{(f)} = |\langle \psi_f^{N-1} | a_j | \psi_0^N \rangle|^2 \tag{8}$$

Note that second quantization[22] has been employed in the latter equation for describing the annihilation of an electron in orbital *j* by means of the operator a_j. Provided all ionization channels can be identified, Feynman−Dyson transition amplitudes and spectroscopic strengths satisfy the following sum rules,

$$\sum_f S_j^{(f)} = 1 \tag{9}$$

$$\sum_f \Gamma_f = N \tag{10}$$

The Kohn−Sham equation[23−26] of DFT may be considered as an approximate quasi-particle equation, with the potential operator approximated by the exchange-correlation potential.[20] We note that there has been a long-standing and vigorous debate on the interpretation of the Kohn−Sham orbital energies as

approximate vertical ionization potentials, for which the current situation is described and improved in ref 24. DFT is often applied with the exchange-correlation (XC) potential represented at the local spin density (LSD) approximation level. In this study we use both the LSD and functionals that depend on the gradients of the electron density,[27−30] i.e., the generalized gradient approximation (GGA). Specifically, here we employed two different approximations to the XC energy functional due to Becke and Perdew (BP)[27−29] and Becke, Lee, Yang, and Parr (BLYP).[27,28,30] However, none of these functionals have the correct Coulombic asymptotic behavior ($-1/r$). Also, Janak's theorem equating ionization energies to KS eigenvalues is only valid for the highest occupied molecular orbital (HOMO). Therefore, any agreement with experimental ionization energies should be viewed as fortuitous. Because Kohn−Sham orbital energies have often been employed to interpret ionization spectra, and are even now used to test the accuracy of extremely sophisticated approaches that incorporate relativistic effects,[31,32] we take this opportunity to emphasize the dangers inherent in such practices. Nonetheless, these same functionals have been shown, for many molecules,[10,11] to provide a good description for the EMS momentum distributions. To further support this latter assertion, we also invoke works by Duffy et al.[33] and Davidson and colleagues[34,35] that demonstrate that KS orbitals most often provide excellent approximations to normalized Dyson orbitals obtained from benchmark quantum mechanical calculations, possibly as the outcome of error cancellations (neglect of final-state correlation, i.e., relaxation effects on orbitals versus the too rapid falloff of the DFT exchange correlation potential at large distances due to the self-interaction error). Gritsenko et al.[25] also notes overlap larger than 0.999 between normalized Dyson orbitals for one-electron ionization events and the corresponding Kohn−Sham orbitals. Thus, presently, the most thorough analyses of EMS are most commonly completed using structure factors derived from KS orbitals derived from DFT calculations employing gradient corrected functionals, along with pole strengths obtained separately from advanced MR−SDCI (multireference single-double configuration interactions[36]) or one-particle Green's function calculations (1p-GF) of the ADC(3) type[37−39] (see further). For this very first analysis of EMS measurements on norbornene, we again apply this very well-established hybrid (1p-GF+DFT) procedure, prior to considering further code developments employing ADC(3) Dyson orbitals for modelling (e,2e) electron momentum distributions.

To compute the coordinate space Kohn−Sham orbitals ψ_j, we employed DGauss, a program package originally developed at CRAY Research by Andzelm and colleagues.[40,41] It has been known for a number of years[42] that HF theory provides momentum distributions of lower quality than DFT due to the lack of electron correlation; therefore we do not assess HF momentum distributions again here. DGauss is itself a part of UniChem.[42] The molecular structure of norbornene has been optimized through energy minimization with various gradient-corrected functionals and basis sets, employing the UniChem user interface. Note that a geometry optimization was performed in DGauss with each basis set used. The electronic structural calculations using a restricted Hartree−Fock (RHF) approach along with a polarized valence basis set of triple-ζ (TZVP) quality are based on GAMESS.[43] A subset of our calculated orbital energies from both our DFT and RHF calculations is given in Table 1b. Clearly none of these results give particularly good agreement with the corresponding experimental values of Table 1a. The reasons for these discrepancies were explored in our recent paper on norbornane,[44] so we do not repeat them again here.

Information of the molecular structure and the molecular orbital wave functions for the ground electronic state of NBN, obtained from the DGauss DFT calculations, were next treated as input to the Flinders-developed program AMOLD,[17] which computes the momentum space spherically averaged molecular-structure factor[19] and the (e,2e) cross section or MD (see eq 3). Note that all the theoretical MDs we report in this paper have had the experimental angular resolution folded in using the method of Frost and Weigold.[45]

The comparisons of calculated MDs with experiment (see section 5) may be viewed as an exceptionally detailed test of the quality of the XC energy and functional and basis set. In this context our LSD, GGA-BP, and GGA-BLYP are used in combination with two basis sets to examine the behavior of the XC functionals and basis sets. These basis sets are denoted by the acronyms DZVP and TZVP. The notations DZ and TZ denote basis sets of double, or triple, ζ quality, respectively. V denotes a calculation in which such a basis is used only for the valence orbitals and a minimal basis is used for the less chemically reactive core orbitals. The inclusion of long-range polarization functions is denoted by P. We note, in particular, that the basis sets of DGauss were specially designed for DFT calculations.[40,46] The TZVP basis set has a contraction scheme [7111/411/1] for carbon and [3111/1] for hydrogen. The auxiliary basis set corresponding to the TZVP basis is called A1,[47] in which the s-, p- and d-orbital exponents were determined separately from an optimization that reproduces, as accurately as possible, the energy from an atomic DFT calculation. The contraction schemes of the A1 basis sets for H are [4/1] and for C [8/4/4].

The DFT DGauss calculations were performed on a Silicon Graphics 02 (R5200) workstation as the UniChem client and a CRAY J90se/82048 computer as the DFT computational engine. A further Hartree−Fock (RHF) calculation, using the TZVP basis set and the GAMESS02 suite of programs,[43] was carried out on the Compaq Alpha Server SC cluster at the Australian Partnership for Advanced Computing National Facilities.

In light of the marginal agreement between the DFT and experimental ionization energies that we described earlier, further calculations employing more sophisticated Green's function techniques were undertaken. These calculations, described in detail in the next section, are all based on geometries[9] that have been optimized using density functional theory[43] employing the TZVP basis set and the nonlocal hybrid Becke three-parameter Lee−Yang−Parr functional (B3LYP).[30,48]

4. Theoretical Analysis of Valence Ionization Spectra

The valence one-electron and 2h−1p (two-hole−one-particle) shake-up ionization bands of norbornene have been calculated using the ADC(3) scheme[49−51] derived within the framework of one-particle Green's function (or one-electron propagator) theory.[52−54] This implies solving a secular problem ($\mathbf{HX} = \mathbf{XE}$, $\mathbf{X}^\dagger\mathbf{X} = \mathbf{1}$) of the form[49−51]

$$\begin{bmatrix} \epsilon + \Sigma(\infty) & \mathbf{U}^{[+]} & \mathbf{U}^{[-]} \\ (\mathbf{U}^{[+]})^\dagger & \mathbf{K}^{[+]} + \mathbf{C}^{[+]} & 0 \\ (\mathbf{U}^{[-]})^\dagger & 0 & \mathbf{K}^{[-]} + \mathbf{C}^{[-]} \end{bmatrix} \begin{bmatrix} \mathbf{X}^1 \\ \mathbf{X}^{2h-1p} \\ \mathbf{X}^{2p-1h} \end{bmatrix} = \begin{bmatrix} \mathbf{X}^1 \\ \mathbf{X}^{2h-1p} \\ \mathbf{X}^{2p-1h} \end{bmatrix} \begin{bmatrix} \mathbf{E}^1 & 0 & 0 \\ 0 & \mathbf{E}^{2h-1p} & 0 \\ 0 & 0 & \mathbf{E}^{2p-1h} \end{bmatrix} \quad (11)$$

At the ADC(3) level, the secular matrix to diagonalize is cast over 1p and excited (shake-on) 2p−1h anionic states [+], as well as over 1h and excited (shake-up) 2h−1p states [−]. In the latter equation, ϵ and $\mathbf{E}^1$ are diagonal matrices containing HF orbital energies and the poles of the 1p-GF correspondingly relating (via a change of sign) to one-electron ionization and electron attachment energies. The 1h and 1p components of the corresponding eigenvectors ($\mathbf{X}^1$) can be related [$(X_j^f)^2 = S_j^{(f)}$] at that theoretical level to the Feynman−Dyson transition amplitudes of eq 8, and from which Dyson orbitals can be expanded as a linear combination of HF orbitals:

$$g_f(\vec{r}) = \sum_j X_j^f \phi_j(\vec{r}) = \sum_j \langle \Psi_f^{N-1} | a_j | \Psi_0^N \rangle \phi_j(\vec{r}) \qquad (12)$$

To achieve a through-third-order treatment of one-electron ionization processes, the block-matrices $\mathbf{K}^{[+]} + \mathbf{C}^{[+]}$ ($\mathbf{K}^{[-]} + \mathbf{C}^{[-]}$) are derived through first-order in correlation as effective configuration interactions between the 2h−1p shake-up (2p−1h shake-on) states. The corresponding shake-up and shake-on energies are contained in the diagonal matrixes $\mathbf{E}^{2h-1p}$ and $\mathbf{E}^{2p-1h}$. The vectors of coupling amplitudes, $\mathbf{U}^{[+]}$ ($\mathbf{U}^{[-]}$) between the 2h−1p (2p−1h) and 1h (1p) states are derived through second-order in correlation. In eq 11, $\Sigma(\infty)$ is the static self-energy describing the electrostatic potential felt by an outgoing or ingoing electron due to correlation corrections to the HF ground-state one-electron density; this potential has been computed through fourth-order in correlation, using charge-consistent one-electron densities.[55]

The ADC(3) calculation, presented in Table 2, was carried out with Dunning's correlation-consistent polarized valence basis set of double-ζ quality (cc-pVDZ[56]), on an ES45 Compaq workstation (4 Gby core memory, 70 Gby disc space, dual processor 677 Mhz) at the University of Hasselt (Belgium). The original code, interfaced to the GAMESS92 package of programs,[43] has been employed to complete these 1p-GF calculations. At the self-consistent field (SCF) level, the requested convergence on each of the elements of the density matrix was fixed to 10^{-10}. With the 1p-GF/ADC(3) approach, the one-hole (1h) and shake-up two-hole−one-particle (2h−1p) ionization energies are recovered through third- and first-order in correlation, respectively, which implies accuracies of ~ 0.2[57] and ~ 0.6 eV on one-electron and shake-up ionization energies, respectively, with a basis set approaching completeness. The spectra have been calculated up to binding energies of 25 eV, retaining all eigenvalues of the ADC(3) secular matrix with a pole strength equal to or larger than 0.005. This matrix has been diagonalized using the Block−Davidson diagonalization procedure[58,59] in the final diagonalization step.[60] The assumption of frozen core electrons has been used throughout and symmetry has been exploited to the extent of the C_s point group. The ADC(3) calculation performed in the present study is based on a molecular geometry that has been optimized using the nonlocal hybrid and gradient corrected Becke three-parameter Lee−Yang−Parr functional (B3LYP)[48,30] in conjunction with Dunning's basis set of triple-ζ quality[61] with polarized valence functions (TZVP). It has previously been shown that this approach delivers excellent equilibrium geometries.[62] For these density functional theory (DFT) computations, the GAUSSIAN98[63] quantum chemistry package has been used.

To evaluate the sensitivity of the computed ionization energies on the quality of the basis set and geometry, a few results (Table 2) were obtained from outer-valence Green's function (OVGF[64,65]) calculations. For these benchmark computations of one-electron ionization energies, three basis sets have been used: Dunning's correlation consistent polarized valence basis set of double-ζ quality (cc-pVDZ[56]), the cc-pVDZ basis augmented by a set of diffuse {s, p} functions on the hydrogen atoms together with a set of diffuse {s, p, d} functions on the carbon atoms (aug-cc-pVDZ[56,66]), and Dunning's correlation consistent polarized valence basis set of triple-ζ quality (cc-pVTZ[56]). The first basis set introduces 148 basis functions for norbornene, the second one 251, and the third one 350, respectively. The results confirm the empirical rule[67] that OVGF pole strengths smaller than 0.85 corroborate a breakdown of the orbital picture of ionization at the ADC(3) level. To examine the influence of the functional and basis set applied in the optimization of the geometry, the molecular structure of norbornene has been further optimized at the B3LYP/cc-pVTZ and MP2/aug-cc-pVDZ theoretical levels (MP2 ≡ Møller−Plesset theory). With respect to the very limited influence (Table 2) on *vertical* one-electron OVGF/cc-pVDZ ionization energies of further improvements of the employed (cc-pVDZ) basis set and (B3LYP/TZVP) geometry ($\sim$0.05 to $\sim$0.1 eV and $\sim$0.02 to $\sim$0.03 eV, respectively), the expected accuracy for the corresponding ADC(3)/cc-pVDZ results is of the order (or better) than $\sim$0.2 eV, which a comparison with the experimental (*adiabatic*) PES (HeI, HeII) values of Table 1 confirms, except for orbital 7a″ ($\sim$0.3 eV discrepancy).

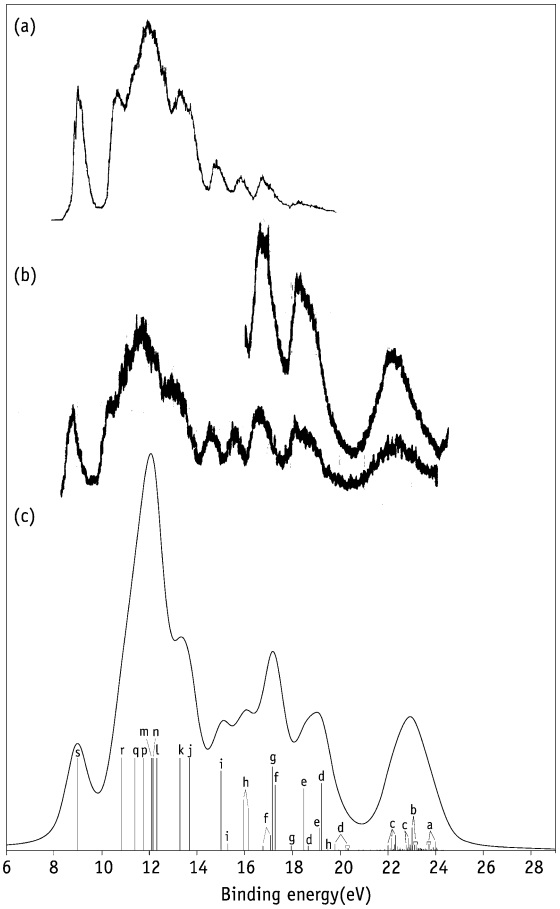

Figure 3. Comparison between the measured (a) He (I),[12] (b) He (II),[15] and [c] ADC(3)/cc-pVDZ theoretical ionization spectrum of norbornene.

As a guide to the eye, the identified solutions of the secular ADC(3) eigenvalue problem are displayed in Figure 3 as a spike spectrum and in the form of a convoluted density of states, along with the ultraviolet photoionization spectra by Bischof et al.[12] and Bieri et al.[15] The convolution has been performed using as a spread function a combination of a Gaussian and a Lorenzian with equal weight with a full width at half maximum (FWHM)

parameter of 1.1 eV and by simply scaling the line intensities according to the computed ADC(3) pole strengths, neglecting thereby the varying influence of molecular orbital cross sections. The comparison between theory and experiment is more than satisfactory for the ionization spectra: our simulations very nicely reproduce the position, shape, width, and relative intensities of bands in the He (I) and He (II) spectra. Note a very significant breakdown of the orbital picture of ionization at binding energies above 22 eV, in the form of a dispersion of the 3a′, 1a″ and 2a′ ionization intensity over many shake-up lines, with comparable strength ($\Gamma_f < 0.225$). No line with a pole strength larger than 0.005 could be recovered for the 1a′ orbital, as a result of the extremely limited symmetry (C_s) of norbornene, which enables many interactions between excited configurations in the cation. By analogy with the 3a′, 1a″, and 2a′ orbitals, and a number of studies of the ionization spectra of *n*-alkanes and cycloalkanes,[67−72] as well as norbornane,[44] we may assume energy relaxation effects of the order of ∼3.5 eV for ionization of an electron out of orbital 1a′. Considering that the HF/cc-pVDZ orbital energy amounts to 31.9 eV, the most important shake-up lines derived from that orbital should therefore concentrate around 28.4 eV, i.e., at ∼4 eV above the vertical double ionization threshold of norbornene which the benchmark CCSD(T)/cc-pVDZ calculations locate at 24.6 eV. 1p-GF studies of ionization spectra using diagonalization approaches that preserve spectral moments,[72] such as the band-Lanczos procedure,[73,74] should be performed to fully confirm this prediction. It is nonetheless clear that all shake-up states that would be identified from such band-Lanczos calculations for the 1a′ orbital are subject to decay via emission of a second electron, and therefore should more correctly be regarded as resonances in a continuum of shake-off states.

5. Comparison between Experimental and Theoretical Momentum Distributions

Deconvolving the ionization spectra, measured at each of a chosen set of angles ϕ, by means of a least-squares fit technique[18] allows us to derive the MDs associated to each of the peaks identified in Figure 2a,b. Although the measured MDs are not absolute, relative magnitudes for the different transitions are obtainable.[17] In the current EMS investigation of the valence states of NBN, the experimental MDs are placed on an absolute scale by summing the experimental flux for each measured ϕ for the first 13 outer-valence orbitals, and then normalizing this to the corresponding sum from our PWIA-BP/TZVP calculation.

The results from this process for the highest occupied molecular orbital (HOMO), the 12a′ orbital, are shown in Figure 4. In this case we find generally good agreement between all the calculated PWIA-XC/TZVP momentum distributions and our corresponding EMS data taken in two independent runs (runs A and B). Agreement between the data and the calculated PWIA-LSD/DZVP momentum distribution is less impressive, but still fair. A slight underestimation of the experimental results by all theoretical methods is noted for $p < 0.8$ au. Significant differences from one model to the other are observed in that momentum region. Note that the error bars on all the MD data represent one standard deviation uncertainty. Further note that the experimental MD data from independent runs A and B are also consistent with one another, a feature that is repeated for all the measured MDs. The results in Figure 4 strongly suggest that the EMS spectroscopic factor (Γ_f) for the 12a′ HOMO is approximately 1. This observation is entirely consistent with our calculated ADC(3) and OVGF spectroscopic factors for this orbital (see Table 2).

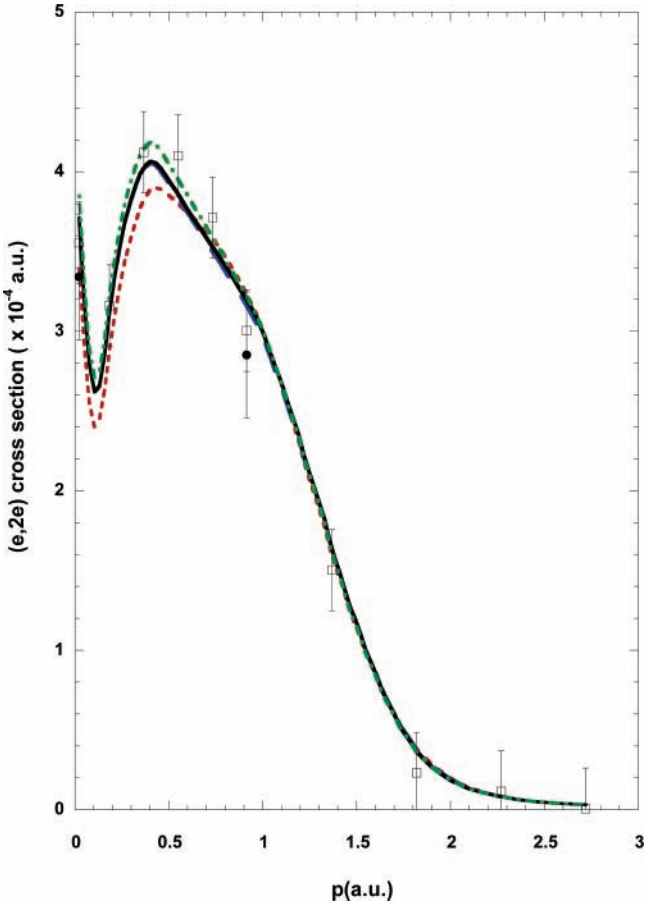

Figure 4. 1500 eV symmetric noncoplanar MD for the 12a′ HOMO of norbornene ($\epsilon_f \sim 8.97$ eV). The present data for run A (●) and run B (□) are compared against the results of our PWIA-DFT calculations: (red - - - -) LSD/DZVP, (blue - -) LSD/TZVP, (black —) BP/TZVP, (green • - • -) BLYP/TZVP. Acronyms are defined in the text.

The HOMO of norbornene has a′ symmetry and, as such, is expected to have a momentum distribution with a nonvanishing and maximal density at $p \rightarrow 0$. This is indeed what is predicted theoretically and observed experimentally (Figure 4). Also in apparently good agreement with the experimental momentum distribution for the HOMO, the peak calculated at $p \rightarrow 0$ is very narrow and followed by a deep minimum at $p \sim 0.1$ au. At larger momenta, the momentum density for the HOMO rises again, to form a second broad distribution with a rather characteristic p-type profile, with a maximum at $p \sim 0.4$ au, and a slight shoulder at $p \sim 1.0$ au. In line with these observations, it is worth noting that, upon large contour values and at close distances (3.5 Å) in the molecular framework, the HOMO can be merely described as a π-type orbital that is strongly localized around the unique C═C bond of this molecule (Figure 5a). This is in sharp contrast with all other orbitals of norbornene (see, for example, Figures 6 and 7 for the NHOMO). This topology at short distances in configuration space explains the very strong resemblance of the corresponding momentum distribution to a p-type profile, at values of p larger than 0.1 au. Upon selecting contour values of 0.008, we see (Figure 5b) that the π-bond starts to interact with much less important contributions from the nearby C−C and C−H bonds. Interestingly, the average radius of the electron density enclosed by this contour is around 7 Å, which corresponds to an electron momentum of 0.0076 au, thus very close to the location of the minimum observed in the MD profile of the HOMO! Upon looking at an extremely low contour value (10^{-8} in Figure 5c

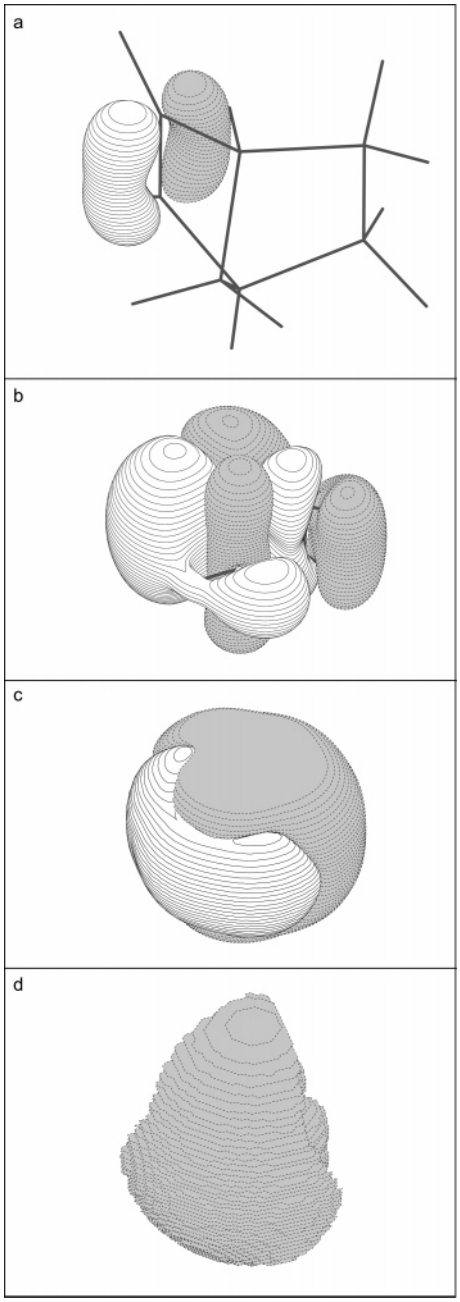

Figure 5. Density contours for the HOMO, using MOLDEN 3.8 and the following inputs: (a) contour = 0.100, edge = 7.00 Å; (b) contour = 0.008, edge = 15.00 Å; (c) contour = 1.00×10^{-8}, edge = 40.00 Å; (d) contour = 5.00×10^{-10}, edge = 200.00 Å (B3LYP/TZVP results).

and 5×10^{-10} in Figure 5d), and correspondingly at very large distances ($r = 20.0$ Å and $r = 100.0$ Å), it appears that the topology of the HOMO reverts to a *s*-type for an external observer. Thus, it can be concluded *that EMS very reliably probes the effective topology of orbitals at varying distances from the molecular center in configuration space, and the way the individual atomic components interact with each other*. In more specific words, the sharp but clearly apparent peak at $p \rightarrow 0$ should be regarded as the consequence at very large distances ($r \rightarrow \infty$) of interferences of the neighboring C−C bonds on the localized π-bond.

Unlike the MD for the HOMO, which exhibits some structure at small *p* (see Figure 4), the measured and calculated MDs for the 7a″ NHOMO all exhibit classic "*p*-like" symmetry.[10] This

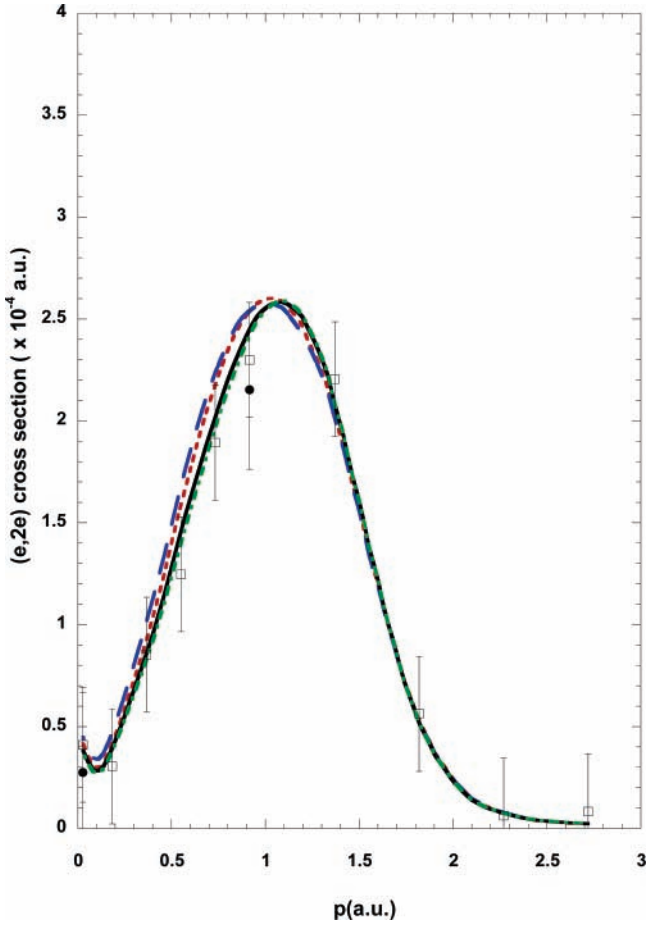

Figure 6. 1500 eV symmetric noncoplanar MD for the 7a″ NHOMO of norbornene ($\epsilon_f \sim 10.55$ eV). The legend is the same as that for Figure 4.

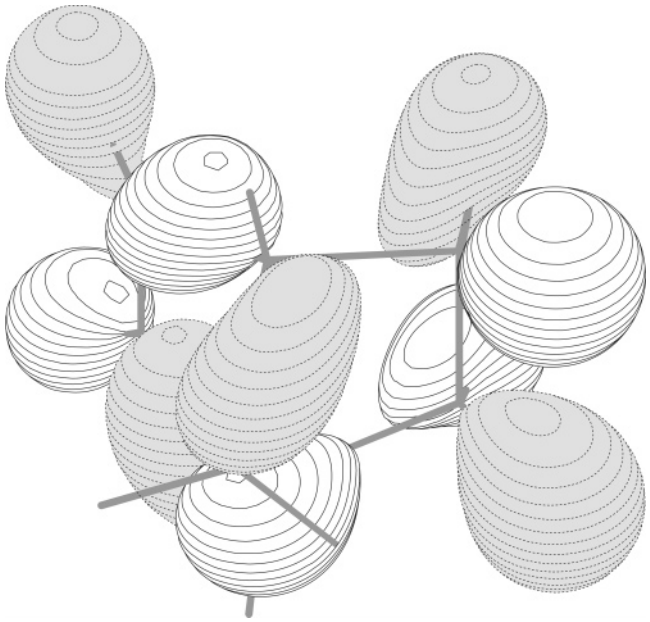

Figure 7. Density contour for the NHOMO, using MOLDEN 3.8 and the following inputs: contour = 0.05, edge = 10.00 Å (B3LYP/TZVP results).

is clearly illustrated in Figure 6. For the NHOMO, however, the PWIA-LSD/DZVP and PWIA-LSD/TZVP calculations slightly overestimate the magnitude of the measured MD. We cannot be more definitive in our comments because of the size of the error bars on the measurement, which largely reflect the

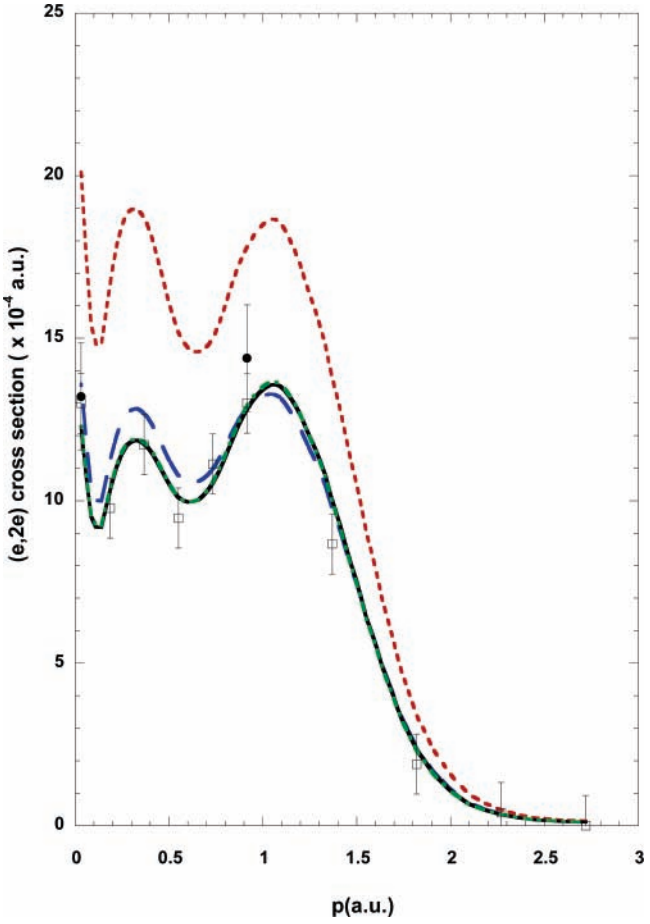

Figure 8. 1500 eV symmetric noncoplanar MD for the 6a″ + 11a′ + 10a′ + 9a′ + 5a″ orbitals of norbornene ($\epsilon_f \sim 11.85$ eV). The legend is the same as that for Figure 4.

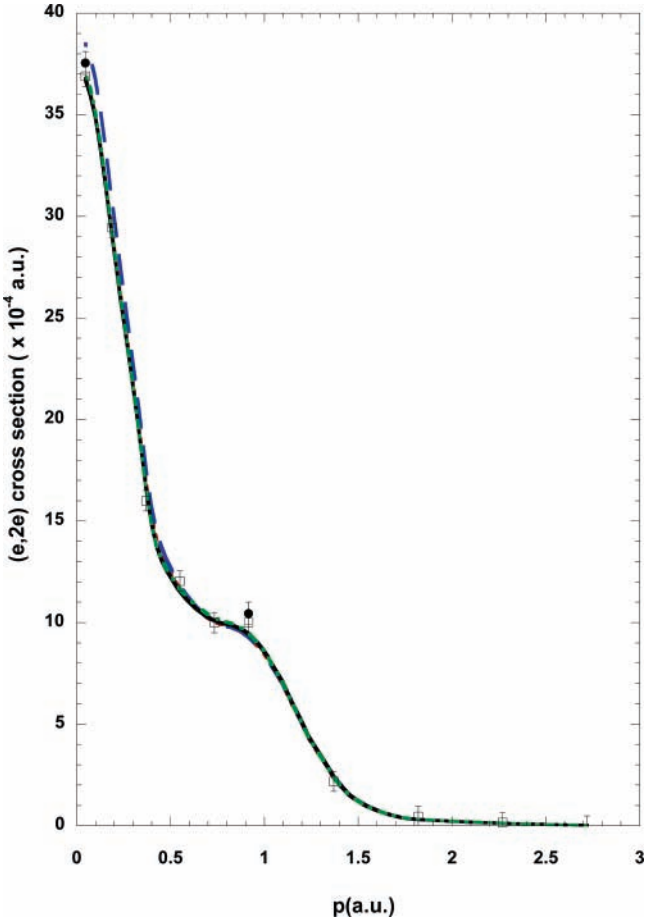

Figure 9. 1500 eV symmetric noncoplanar MD for the 5a′ + 3a″ orbitals of norbornene ($\epsilon_f \sim 16.71$ eV). The legend is the same as that for Figure 4.

relatively small (e,2e) cross section for this orbital. Agreement between the measured MD and the calculated PWIA-BP/TZVP and PWIA-BLYP/TZVP momentum distributions remains excellent. As was the case for the HOMO, the results in Figure 6 also strongly suggest that $\Gamma_{7a''}^{EMS} \sim 1$, which is again in good accord with our calculated ADC(3) and OVGF pole strengths (see Table 2). Finally, from inspection of the density contours drawn for the NHOMO (see Figure 7), we note that this orbital clearly contributes to the σ_{C-C} and σ_{C-H} bond systems of norbornene.

In Figure 8 we show the measured and calculated MDs for the 6a″ + 11a′ + 10a′ + 9a′ + 5a″ orbitals of norbornene. Recall that combining the MDs of all these orbitals was necessary due to the limited experimental energy resolution. For these orbitals we find that the momentum distribution calculated at the LSD/DZVP level, within the plane wave impulse approximation (PWIA), significantly overestimates the magnitude of the experimental cross section for all p. This suggests that the combination of the LSD exchange correlation functional and DZVP basis set is not providing a very good representation of these orbitals. Though less striking, Figure 8 also appears to indicate for momenta in the range 0.15 au $\leq p \leq$ 0.75 au that the PWIA-LSD/TZVP momentum distribution overestimates the magnitude of the experimental MD. Nonetheless, the very good level of agreement between theory and experiment for the remaining BP/TZVP and BLYP/TZVP results shows that the EMS spectroscopic factors for all the 6a″, 11a′, 10a′, 9a′, and 5a″ orbitals probably lie within the range 0.9−1. This finding is consistent with the MO picture of ionization being valid here for these outer-valence orbitals, a result in good agreement with our ADC(3) and OVGF calculations of Table 2. The momentum distribution shown in Figure 8 exhibits three maxima and two minima, which presumably reflects the fact that the corresponding set of orbitals contain two *p*-type (a″) and three *s*-type (a′) orbitals, hence the nonvanishing contribution at $p = 0$ au.

The 5a′ + 3a″ orbital momentum distributions are illustrated in Figure 9. In this case we see that all the MDs are strongly peaked (large cross section) as $p \rightarrow 0$ au, indicating an "s-type" symmetry[10] probably due to strong C(2s) contributions. However, it is also clear from Figure 9 that there is an important structure in the MDs, occurring at around $p \sim 0.9$ au. This indicates there is also a "p-type" contribution[10] to the overall symmetry of the MDs, due to orbital 13 (3a″). In all cases we find very good agreement between the experimental and theoretical MDs for these orbitals, suggesting that the 5a′ + 3a″ orbitals do not provide a very sensitive test for the quality of our various PWIA-XC/DFT calculations. From the data in Figure 9 we estimate our (total) EMS spectroscopic factors for the 5a′ and 3a″ orbitals would be in the range 0.9−1, which is consistent with the fractions of intensity recovered under the form of lines with a spectroscopic strength larger than 0.005 and which amount to 0.881 and 0.842, respectively. Note, nonetheless, a shake-up satellite originating from ionization of the 3a″ orbital with a rather significant intensity ($\Gamma_f = 0.151$) at 17.1 eV, which EMS cannot discriminate from the main (one-electron) ionization line at 17.3 eV because of the too limited experimental resolution.

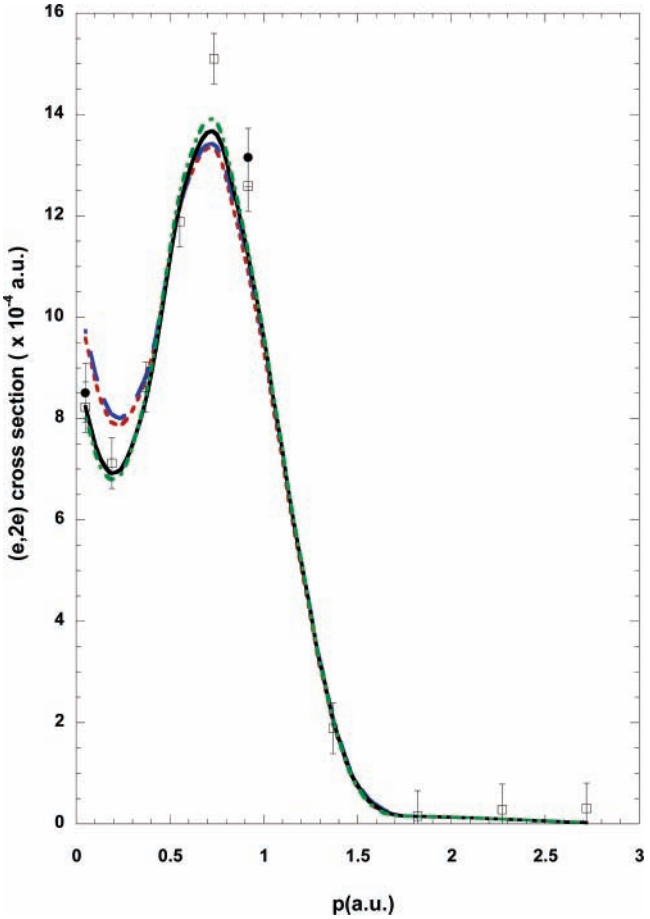

Figure 10. 1500 eV symmetric noncoplanar MD for the 4a′ + 2a″ orbitals of norbornene ($\epsilon_f \sim 18.22$ eV). The legend is the same as that for Figure 4.

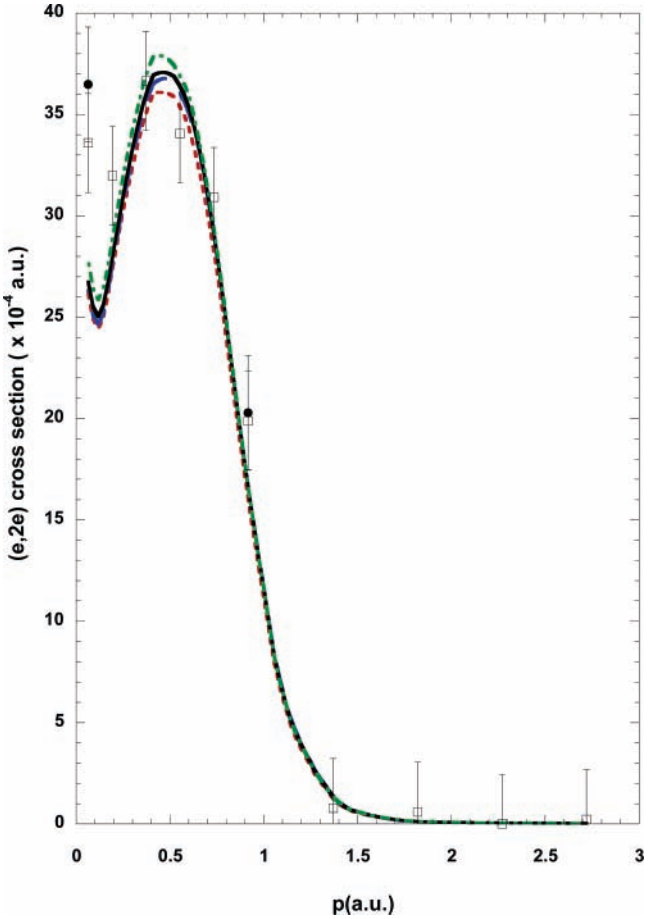

Figure 11. 1500 eV symmetric noncoplanar MD for the 3a′ + 1a″ + 2a′ orbitals of norbornene. The legend is the same as that for Figure 4.

The MD shown in Figure 10 displays two maxima at $p \sim 0$ au and $p = 0.75$ au, along with one minimum at 0.2 au. This undoubtedly reflects the fact that the analyzed set of orbitals (4a′ + 2a″) contain one s-type (4a′) orbital and one p-type (2a″) orbital. In this case the superiority of the PWIA-BP/TZVP and PWIA-BLYP/TZVP MDs, for $p < 0.4$ au, is clear. However, none of the theoretical MDs correctly reproduces the experimental MD over the entire range of p studied. The theoretical MDs seem to underestimate the magnitude of the peak in the (e,2e) cross section in the vicinity of $p \sim 0.75$ au, and none of the calculated MDs correctly predict the width of this peak. This is precisely the reason we seek an "optimum" wave function for the molecule in question. It is quite rare in EMS for theory to be able to accurately predict all the experimental MDs for all the MOs in question.[10,11] For norbornene we have seen that both the PWIA-BP/TZVP and PWIA-BLYP/TZVP calculations do a reasonable job in reproducing the experimental MDs for most of the orbitals considered. For norbornene, however, unlike some previous species,[11] it is hard to state which model wave function works best overall. As a consequence, we must rely on the experience acquired with our previous studies of chemically similar species such as norbornane[44] and norbornadiene.[75] In those two cases the BP/TZVP exchange correlation functional and basis set best represented these species, and as a consequence we also choose BP/TZVP as our "optimum" model for norbornene. Before discussing the molecular geometry of norbornene, derived from BP/TZVP, let us consider the most challenging part of the ionization spectrum, namely the innermost valence region at $\epsilon_f \geq 25$ eV.

The cumulative momentum distribution for orbitals 3a′, 1a″, and 2a′ is displayed in Figure 11. As for the $2a_1 + 1b_2 + 1b_1$ orbitals of norbornane,[44] the theoretical momentum distributions, whatever the employed model chemistry, are somewhat lower in magnitude than the experimental ones, especially at $p < 1$ au. Nonetheless, the present experimental momentum profile exhibits clearly a minimum at $p \sim 0.2$ au, in fair agreement with theory, and thus nicely reflects the fact that bands 9 and 10 consist of a mixture of ionization lines with s-type and p-type symmetries. The underestimation by theory of the experimental EMS cross sections at low momenta can be attributed to a number of shortcomings in the employed model, among others being the well-known deficiencies of the currently used gradient corrected BP functional in the asymptotic region ($r \rightarrow \infty$), or significant departures from a vertical depiction of ionization due to ultrafast molecular relaxation and nuclear dynamical effects in a highly strained cage structure, at shake-up ionization energies approaching the double ionization threshold (24.6 eV; see above). By analogy with ref 76, one may of course also always invoke a breakdown of the plane wave impulse approximation—we would like to emphasize, however, that it may not be appropriate to systematically and only blame failings in that approximation as soon as Kohn−Sham (BP) momentum distributions for vertical ionization events fail to quantitatively reproduce experiment. In line with this, we suggest for instance that the strong dependence of the relative (e,2e) cross sections at very small momenta, on the energy of the impinging electron, that was recently observed in EMS experiments on glyoxal,[77] might not (only) be due to shortcomings in the PWIA. Rather, it might also reflect changes of the time scale of the (e,2e)

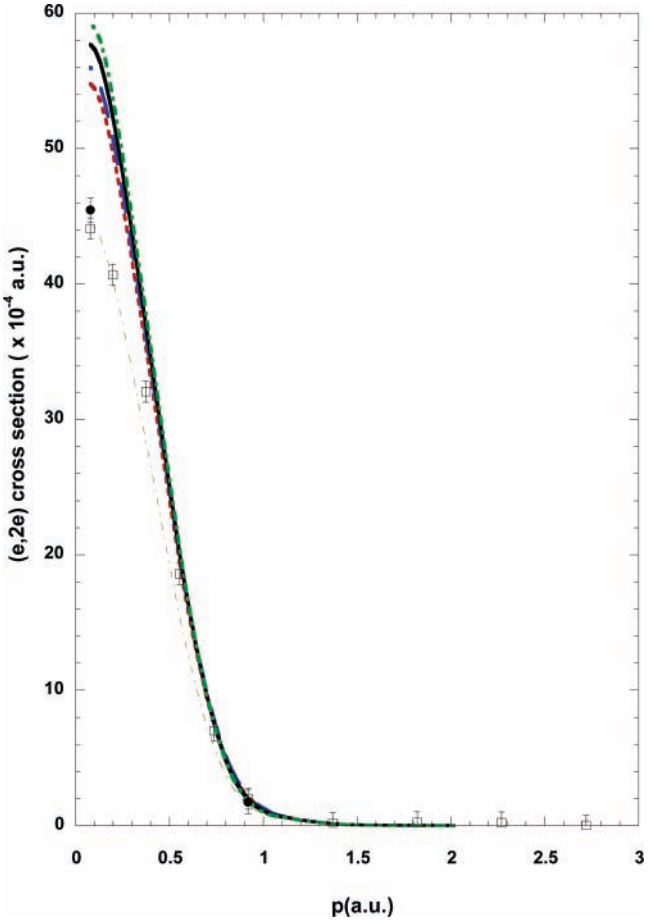

Figure 12. 1500 eV symmetric noncoplanar MD for the innermost valence orbital (1a′) of norbornene. The legend is the same as that for Figure 4, except an additional MD representing 0.77 × PWIA-BP/TZVP result (thin dash-dot line) is also plotted.

ionization processes ($\sim 10^{-17}$ s[78]). In other words, this energy dependence may reflect variations of the extent of the nuclear motions that are effectively probed in these experiments. Figure 12 illustrates the experimental MD for the sum of peaks 11 and 12 of Figure 2, and the corresponding 1a′ theoretical MDs from the models considered. All the theoretical MDs do a fair job in predicting the shape of the experimental result, although they all overestimate the magnitude of the experimental cross section over most of the measured momentum range. This result is not really surprising as it is clear from Figure 2 that there is additional experimental flux at binding energies greater than 30 eV, which we are not accessing in this study. When our PWIA-BP/TZVP momentum distribution for the 1a′ orbital is scaled by a factor of 0.77, fair agreement is found between the experimental MD for peaks 11 and 12 and this scaled theory result. This provides further justification for our preliminary assignment of the measured flux originating from ionization of the 1a′ orbital. However, as our ADC(3) result does not find any ionization line for the 1a′ orbital with a pole strength larger than 0.005, our assignment must remain tentative at this time. We would advocate again further band-, or block-Lanczos studies of the bands relating to shake-up lines with a pole strength smaller than 0.005.

Finally, we note that there are several orbital MDs that we have not specifically been discussed or plotted in this section. Plots of these MDs are available on request to one of the corresponding authors (M.J.B.). These MDs reinforce the argument for the utility of either BP/TZVP or BLYP/TZVP that we have made in this section but do not add any further insight.

6. Molecular Properties of Norbornene

6.1. Molecular Geometry. We used the BP/TZVP model to derive the molecular structure of norbornene. This was compared in detail with experimentally determined values[79−81] and those from other MO calculations[1,9,81,82] to determine how well the BP/TZVP model reproduced the structure.

In general, our calculations of molecular geometries using the BP/TZVP model are in very good agreement with the experimentally determined molecular geometries (given the experimental uncertainties) and compare favorably with the results from other MO calculations. The results are summarized in Table 3. Note that in Table 3 we have only included the highest-level calculation reported by Holthausen and Koch[82] and have omitted the recent calculations on the structural impact on the methano-ring in norbornadiene, norbornene, and norbornane by Wang et al.[9] as they originate from our group. To assist the reader in the discussion that follows, refer to the structural representation and atom numbering of the norbornene molecule that we gave in Figure 1.

The C_5-C_6 single bond involving two of the methylene carbon atoms has a bond distance of 1.560 Å from our calculations, in excellent agreement with that from the recent synchrotron radiation powder diffraction study[81] and also in good agreement with those from the earlier electron diffraction[79] and X-ray powder diffraction[80] studies. The $C_2=C_3$ double bonded methylene carbons have a bond length of 1.348 Å from our BP/TZVP calculation, in fair agreement with all the experimental results[79,80] when their respective uncertainties are allowed for. The remaining carbon−carbon bonds involving the bridge or bridgehead carbon atoms are also in excellent agreement with experiment (see Table 3). The agreement with experiment for our BP/TZVP calculation is better than for the small basis set ab initio and semiempirical MO-derived geom-

TABLE 3: Experimental and Theoretical Molecular Geometry of Norbornene

parameter	gas phase electron diffraction[79]	X-ray powder diffraction[80]	synchrotron radiation powder diffraction[81]	BP/TZVP present	HF/STO-3G[1]	HF/6-31G* [81]	MP2/6-311G(d)
$r(C_1-C_6)$ Å	1.550	1.562	1.558	1.571	1.563	1.558	1.561
$r(C_1-C_7)$ Å	1.566	1.547	1.543	1.550	1.548	1.541	1.540
$r(C_5-C_6)$ Å	1.556	1.556	1.560	1.560	1.556	1.559	1.555
$r(C_2-C_3)$ Å	1.336	1.334	1.332	1.348	1.314	1.324	1.351
$r(C_1-C_2)$ Å	1.529	1.524	1.524	1.524	1.535	1.523	1.515
$\angle C_1C_5C_6$, deg	−	100.5	103.5	102.98	102.9	102.7	−
$\angle C_1C_7C_4$, deg	−	92.3	95.3	93.78	93.3	93.5	94.0
$\angle C_2C_1C_6$, deg	−	109.3	105.6	105.87	106.4	106.5	−
$\angle C_2C_1C_7$, deg	−	99.4	99.0	100.29	100.9	100.5	−
$\angle C_6C_1C_7$, deg	−	102.1	99.6	100.32	99.4	100.0	−
$\angle C_1C_2C_3$, deg	108.6	106.5	108.1	107.45	107.8	107.6	107.3
d(C2−C6) Å	−	−	−	2.470	−	−	−

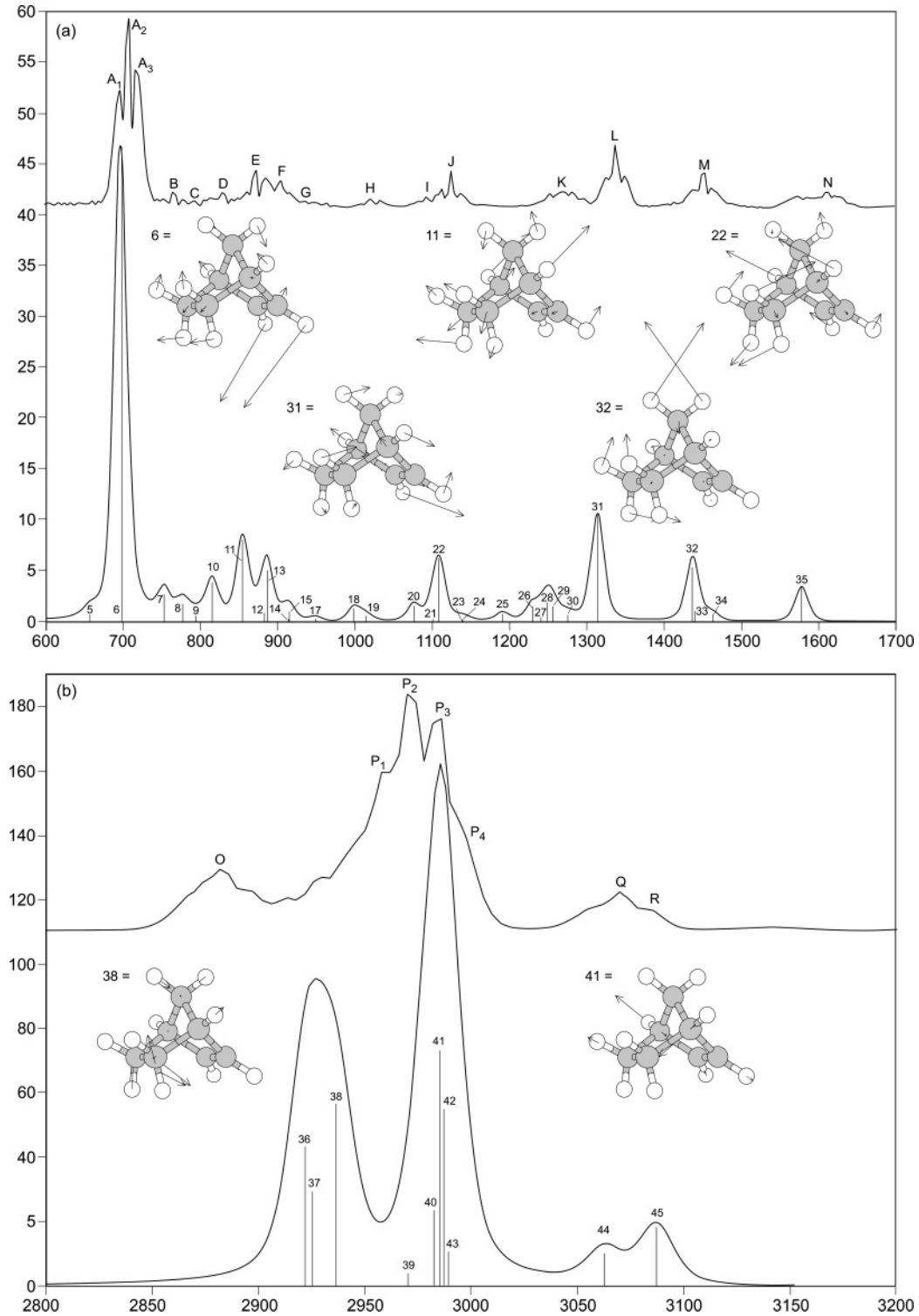

Figure 13. Experimental[85] and BP/TZVP simulation for the vibrational spectra of norbornene: (a) 600−1700 cm^{-1} (b) 2800−3200 cm^{-1}. Note that the theory is convolved with a 20 cm^{-1} (FWHM) Gaussian. Note also that the most apparent vibrational eigenmodes are displayed in this figure (see Table 4 for label definitions).

etries in Table 3,[1,81,82] although we note that the second-order Møller/Plesset perturbation theory (MP2) result from Holthausen and Koch[82] is also doing a fair overall job.

The experimental bond angles were also in general well reproduced by our BP/TZVP calculation, especially the bridge and bridgehead angles. The bridge angle ($\angle C_1C_7C_4$) of 93.78° from our DFT calculation lies comfortably within the experimental range of 92.3−95.3° from the X-ray and synchrotron powder diffraction studies,[79,80] respectively. A similar result can be found for nearly all the other bond angles we list in Table 3; namely our DFT result lies comfortably within the spread of angles represented by the various experimental investigations,[79−81] except for $\angle C_2C_1C_7$, which the BP/TZVP approach tends to slightly overestimate as compared with the experimental results.

6.2. Vibrational Spectra. In the present work, we also make use of the BP/TZVP model that has been previously calibrated against experimental momentum distributions in a study of the infrared (IR) spectrum of norbornene, employing the harmonic oscillator approximation for computing

TABLE 4: Theoretical Analysis of the IR Spectrum of Norbornene[a]

		BP/TZVP		B3LYP/TZVP		MP2/aug-cc-pVDZ		experiment[b]			
mode number	symmetry label	freq	int	freq	int	freq	int	peak	freq	max int[c]	int abs[d]
1	a″	246.8	0.0	258.8	0.0	241.5	0.0				
2	a′	366.5	3.1	382.1	2.6	372.6	3.1				
3	a′	460.8	1.3	479.2	1.1	467.9	1.2				
4	a″	471.8	0.2	487.9	0.2	471.7	0.2				
5	a″	656.7	0.7	677.9	0.6	661.8	0.6	A_1	698.0	16.25	
6	a′	697.9	46.6	730.0	41.4	713.9	45.4	A_2	710.0	26.02	16.98
								A_3	718.0	19.11	
7	a′	753.1	2.7	775.7	2.5	773.3	4.9	B	766.0	2.680	0.625
8	a″	777.1	1.8	799.0	1.8	794.5	0.9	C	790.0	1.480	0.426
9	a′	794.1	0.6	821.9	0.5	813.4	0.4				
10	a″	815.0	3.9	836.6	2.8	844.2	3.8	D	830.0	2.610	1.395
11	a′	854.7	8.0	878.1	7.3	891.5	5.6	E	874.0	5.530	1.244
12	a′	882.6	1.0	904.9	0.8	922.5	0.9				
13	a″	886.6	5.1	916.5	3.0	900.5	4.3	F	906.0	4.200	1.368
14	a″	914.0	0.5	959.2	1.1	947.4	0.3				
15	a′	914.5	1.1	938.7	1.2	956.8	0.0	G	938.0	1.400	0.435
16	a″	935.3	0.0	966.2	0.7	960.7	0.5				
17	a′	949.2	0.4	972.8	0.6	982.6	0.4				
18	a′	999.0	1.4	1038.3	1.3	1028.8	1.0	H	1022.0	1.710	0.533
19	a″	1014.9	0.7	1055.1	0.9	1033.4	0.4				
20	a′	1076.5	1.6	1116.2	1.2	1098.7	1.3	I	1098.0	1.590	0.948
21	a″	1100.5	0.3	1139.8	0.4	1121.1	0.2				
22	a′	1108.6	6.2	1148.0	4.9	1133.4	4.8	J	1126.0	5.230	2.706
23	a″	1138.8	0.2	1184.7	0.2	1171.3	0.1				
24	a′	1139.8	0.2	1188.2	0.2	1167.0	0.1				
25	a″	1191.0	0.8	1238.3	0.5	1223.2	0.6				
26	a″	1229.9	1.5	1285.8	1.7	1253.6	0.9				
27	a″	1240.5	0.4	1297.1	0.0	1267.8	0.4				
28	a″	1248.9	1.9	1301.5	1.1	1283.8	2.1	K	1270.0	2.620	3.143
29	a′	1256.2	1.4	1305.8	1.1	1296.0	1.7				
30	a′	1275.6	0.6	1329.6	0.4	1309.5	0.2				
31	a″	1313.9	10.5	1367.2	9.9	1354.7	7.2	L	1338.0	8.670	4.932
32	a′	1436.3	5.3	1494.2	4.4	1470.7	4.6	M	1454.0	5.090	4.231
33	a″	1439.6	1.0	1495.2	0.9	1473.1	0.8				
34	a′	1462.5	0.7	1517.8	0.7	1497.9	0.7				
35	a′	1578.0	3.3	1636.3	2.4	1586.3	3.2	N	1610.0	2.500	4.036
36	a′	2966.5	43.3	3040.6	41.1	3068.7	36.6				
37	a″	2969.8	29.4	3042.4	27.3	3073.7	25.9				
38	a′	2981.3	56.4	3054.8	56.5	3085.7	49.3	O	2882.0	26.41	19.54
39	a″	3015.6	4.0	3082.8	4.4	3135.1	4.1				
40	a′	3027.8	23.7	3096.8	26.0	3144.1	7.9	P_1	2958.0	67.11	
41	a″	3030.7	73.3	3100.2	76.5	3141.8	58.7	P_2	2970.0	100.0	100.0
42	a′	3032.7	55.1	3101.2	57.0	3148.6	23.5	P_3	2986.0	89.66	
43	a′	3034.8	10.7	3104.8	12.5	3152.5	45.2	P_4	2990.0	54.76	
44	a″	3109.3	10.3	3181.4	9.8	3218.6	6.9	Q	3070.0	16.73	11.72
45	a′	3134.2	18.2	3205.9	18.0	3244.6	15.6	R	3142.0	19.00	2.012

[a] Frequencies and calculated intensities are given in cm^{-1} and km/mol, respectively. [b] See ref 85. [c] Relative intensity in arbitrary unit at peak maximum. [d] Integrated absorbency in arbitrary unit.

vibrational eigenstates. Electrical harmonicity is further invoked to compute IR frequencies as functions of mixed second-order derivatives of the total energies with respect to normal displacements and to an external electric field (the so-called double harmonic approximation[83,84]). The obtained results are provided in Figure 13, using as a spread function for convolving the spike spectrum a Gaussian of 20 cm^{-1} full width at half the maximum. Along with the experimental spectrum[85] and the BP/TZVP simulation, the most apparent vibrational eigenmodes are also displayed in Figure 13. The simulation in Figure 13b for the frequency range comprised between 2800 and 3200 cm^{-1} has been drawn using for the sake of clarity a rescaling factor of 0.985 on frequencies, whereas *unrescaled* frequencies have been used for Figure 13a (600−1700 cm^{-1}).

With the BP/TZVP model, we have been able to reproduce the position of the bands in the experimental spectrum (Figure 13, Table 4) with reasonable accuracy (about ∼27 cm^{-1} on average). A rather noteworthy exception is band O at 2880 cm^{-1}, which, whatever the level, theory systematically overestimates by 100−200 cm^{-1} (Table 4). It is thus worth noting that the BP/TZVP results are also in line with B3LYP/cc-pVTZ and MP2/aug-cc-pVDZ calculations (Table 4), except for an energy reordering of a few pairs of nearly degenerate lines, within energy intervals of the order of a few cm^{-1}, and which can therefore not be resolved experimentally. Relative intensities of bands are also nicely reproduced (Figure 13), taking into account the fact that rotational transitions may differently broaden bands. Rotational levels with a characteristic energy spacing of about 10 cm^{-1} are for instance very clearly apparent on the experimental side in the bands (**A**, **P**) associated to the vibrational eigenmodes **6** and **39**−**43**, which both relate to rather strongly localized distortions, namely the H−C═C out-of-plane bending and C−H stretching modes, respectively (Figure 13). The other modes (Figure 13) are more delocalized and quite naturally therefore exhibit a lesser IR intensity.

Superficially it appears that, among the retained BP/TZVP, B3LYP/cc-pVTZ, and MP2/aug-cc-pVDZ models, BP/TZVP

is the one that provides the most accurate insights into the IR spectrum of norbornene. Some care is needed, however, before concluding that BP/TZVP is the best model for IR spectroscopy: indeed, due to the neglect of anharmonicities, theoretical frequencies obtained on the basis of the RRHO approximation are expected to overestimate the experimental ones by typically a few percent, and this is precisely what is observed at the B3LYP/cc-pVTZ and MP2/aug-cc-pVDZ levels. Due to the importance of cyclic strains in the investigated cage compounds, we expect that anharmonicities should have an unusually strong influence on the frequencies. In sharp contrast with the normal expectations, the BP/TZVP frequencies in the 600−1700 cm^{-1} frequency range are found to systematically *underestimate* experimental values by ∼20 cm^{-1}. In line with our previous comments on the need to develop ab initio schemes for computing orbital momentum distributions from benchmark Dyson orbital theories, this indicates that the superiority of the BP/TZVP//RRHO model in reproducing experimental frequencies is very probably the outcome of error cancellations. This model is obviously sufficient for assigning vibrational bands with great confidence, but clearly, further models fully coping with anharmonic effects, centrifugal distortions, employing huge basis sets (at least aug-cc-pVTZ), and last but not least, treating electronic correlation at an extremely high-level (CCSD[T]) will be needed before stating that the right frequencies have been obtained for the right reasons, within 20 cm^{-1} accuracy. Such calculations, however, are far too computationally expensive to be performed at present.

7. Conclusions

We have reported on the first comprehensive EMS study of the valence electronic structure of norbornene, in conjunction with DFT calculations of orbital MDs, and 1p-GF (OVGF and ADC(3)) calculations of the one-electron and shake-up ionization spectrum. Very good agreement is generally found between the experimental PES and EMS binding energies, on one hand, and the 1p-GF results, on the other hand. Where a comparison is possible, pole strengths calculated by our 1p-GF procedures, certainly for the outer valence orbitals, were found to be largely consistent with those determined from our EMS MD data. Strong final state configuration interaction effects are predicted in our ADC(3) calculation for the inner valence 3a′, 1a″, 2a′, and 1a′ orbitals, a prediction which is consistent with the very significant band broadening observed at binding energies beyond ∼20 eV.

Momentum distributions for the 12a′, 7a″, 6a″ + 11a′ + 10a′ + 9a′ + 5a″, 4a″ + 8a′, 7a′, 6a′, 5a′ + 3a″, 4a′ + 2a″, 3a′ + 1a″ + 2a′, and 1a′ orbitals were measured and compared against a series of PWIA-based calculations using DFT DGauss basis sets. Our calculations, for each of the two basis sets (DZVP and TZVP), were performed using LSD and both BP and BLYP exchange correlation corrections to the DFT functional. On the basis of this comparison between the experimental and theoretical MDs, and on our previous experience with the series of structurally similar species of norbornadiene (NBD) and norbornane (NBA),[75,44] we found that BP/TZVP provided an acceptable representation of the experimentally determined NBN wave function. The molecular structure of norbornene, as derived from this "optimum" BP/TZVP wave function, was seen to be in generally good agreement with the results from independent measurements. This provides compelling evidence for the utility of EMS in a priori evaluation of a quantum chemical wave function. In future works, with respect to the known limitations of currently available gradient corrected functionals, the quality of model wave functions derived from DFT computations should also be tested in detail against Dyson orbitals obtained from benchmark 1p-GF/ADC(3) calculations. The consequences of both electronic and molecular relaxation effects and nuclear dynamics within the time scale of EMS should in the future also be examined systematically in detail.

The present study is the final in a series that looked at the chemically similar molecules NBD,[75] NBN, and NBA.[44] Although a preliminary report into how the valence electronic structure of these molecules changes as the double bonds of NBD are progressively saturated has been made,[9] a detailed analysis of the sensitivity of the respective momentum distributions to these bonding changes has yet to be made. Such a review is foreshadowed here, although no further details are given at this time.

Acknowledgment. This work was supported in part by the Australian Research Council, and we thank Ms. Marilyn Mitchell for typing the manuscript. K.L.N. thanks the Ferry Trust for her scholarship, and F.W. acknowledges the Australian Partnership for Advanced Computing (APAC) for use of their facilities. M.S.D., S.K., and J.P.F. acknowledge financial support from the Bijzonder Onderzoeks Fonds (BOF) of the Universiteit Hasselt, previously known as Limburgs Universitair Centrum, and from the Fonds voor Wetenschappelijk Onderzoek_Vlaanderen (FWO), the Flemish Branch of the National Scientific Foundation of Belgium.

Note Added after ASAP Publication. This article was released ASAP on September 2, 2005. Additional changes have been incorporated throughout the paper after the manuscript was posted on the Web. The correct version was posted on September 28, 2005.

References and Notes

(1) Castro, C. R.; Dutler, R.; Rauk, A.; Wieser, H. *J. Mol. Struct. (THEOCHEM)* **1987**, *152*, 241.
(2) Koga, N.; Ozawa, T.; Morokuma, K. *J. Phys. Org. Chem.* **1990**, *3*, 519.
(3) Spanget-Larsen, J.; Gleiter, R. *Tetrahedron* **1983**, *39*, 3345.
(4) Rondan, N. G.; Paddon-Row, M. N.; Caramella, P.; Houk, K. N. *J. Am. Chem. Soc.* **1981**, *103*, 2436.
(5) Spanget-Larsen, J.; R Gleiter, R. *Tetrahedron Lett.* **1982**, *23*, 2435.
(6) Wilsey, S.; Houk, K. N.; Zewail, A. H. *J. Am. Chem. Soc.* **1999**, *121*, 5772.
(7) Diels, O.; Alder, K. *Justus Liebigs Ann. Chem.* **1928**, *460*, 98.
(8) Dewar, M. J. S.; Jie, C. *Acc. Chem. Res.* **1992**, *22*, 537.
(9) Wang, F.; Brunger, M. J.; Winkler, D. A. *J. Phys. Chem. Sol.* **2004**, *65*, 2041.
(10) Weigold, E.; McCarthy, I. E. *Electron Momentum Spectroscopy*; Kluwer Academic/Plenum Publishers: New York, 1999.
(11) Brunger, M. J.; Adcock, W. *J. Chem. Soc., Perkin Trans.* **2002**, *2*, 1.
(12) Bischof, P.; Hashmall, J. A.; Heilbronner, E.; Harnung, V. *Helv. Chim. Acta* **1969**, *52*, 110.
(13) Demeo, D. A.; Yencha, A. J. *J. Chem. Phys.* **1970**, *53*, 4536.
(14) Wen, A. T.; Hitchcock, A. P.; Werstiuk, N. H.; Nguyen, N.; Leigh, W. J. *Can. J. Chem.* **1990**, *68*, 1967.
(15) Bieri, G.; Burger, F.; Heilbronner, E.; Maier, J. P. *Helv. Chim. Acta* **1977**, *60*, 2213.
(16) Bodor, N.; Dewar, M. J. S.; Worley, S. D. *J. Am. Chem. Soc.* **1970**, *92*, 19
(17) McCarthy, I. E.; Weigold, E. *Rep. Prog. Phys.* **1991**, *54*, 789.
(18) Bevington, P. R.; Robinson, D. K. *Data Reduction and Error Analysis for the Physical Sciences*; McGraw-Hill Inc.: New York, 1990.
(19) McCarthy, I. E.; Weigold, E. *Rep. Prog. Phys.* **1988**, *51*, 299.
(20) Casida, M. *Phys. Rev. A* **1995**, *51*, 2005.
(21) Deleuze, M. S.; Pickup, B. T.; Delhalle, J. *Mol. Phys.* **1994**, *83*, 655.
(22) Szabo. A.; Ostlund, N. S. *Modern Quantum Chemistry: Introduction to Advanced Electronic Structure Theory*; McGraw-Hill: New York, 1989.
(23) Kohn, W.; Sham, L. J. *Phys. Rev.* **1965**, *140*, A1133.

(24) Chong, D. P.; Gritsenko, O. V.; Baerends, E. J. *J. Chem. Phys.* **2002**, *116*, 1760.
(25) Gritsenko, O. V.; Braida, B.; Baerends, E. J. *J. Chem. Phys.* **2003**, *119*, 1937.
(26) Jellinek, J.; Acioli, P. H. *J. Chem. Phys.* **2003**, *118*, 7783.
(27) Becke, A. D. *Phys. Rev. A* **1988**, *38*, 3098.
(28) Becke, A. D. *J. Chem. Phys.* **1988**, *88*, 2547.
(29) Perdew, J. P. *Phys. Rev. B* **1986**, *33*, 8822.
(30) Lee, C.; Yang, W.; Parr, R. G. *Phys. Rev. B* **1988**, *37*, 785.
(31) Liu, W.; Hong, G.; Dai, D.; Li, L.; Dolg, M. *Theor. Chem. Acc.* **1997**, *96*, 75.
(32) Choi, Y. J.; Lee, Y. S. *J. Chem. Phys.* **2003**, *119*, 2014.
(33) Duffy, P.; Chong, D. P.; Casida, M. E.; Salahub, D. R. *Phys. Rev. A* **1994** *50*, 4707.
(34) Davidson, E. R. *Can. J. Phys.* **1996**, *74*, 757.
(35) Rolke, J.; Zheng, Y.; Brion, C. E.; Chakravorty, S. J.; Davidson, E. R.; McCarthy, I. E. *Chem. Phys.* **1997**, *215*, 191.
(36) Zheng, Y.; Pang, W. N.; Shang, R. C.; Chen, X J.; Brion, C. E.; Ghanty, T. K.; Davidson, E. R. *J. Chem. Phys.* **1999**, *111*, 9526.
(37) Pang, W. N.; Gao, J. F.; Ruan, C. J.; Shang, R. C.; Trofimov, A. B.; Deleuze, M. S. *J. Chem. Phys.* **2000** *112*, 8043.
(38) Deleuze, M. S.; Pang, W. N.; Salam, A.; Shang, R. C. *J. Am. Chem. Soc.* **2001**, *123*, 4049.
(39) Adcock, W.; Brunger, M. J.; McCarthy, I. E.; Michalewicz, M. T.; von Niessen, W.; Wang, F.; Weigold, E.; Winkler, D. A. *J. Am. Chem. Soc.* **2000**, *122*, 3892.
(40) Andzelm, J.; Wimmer, E. *J. Chem. Phys.* **1992**, *96*, 1290.
(41) Komornicki, A.; Fitzgerald, G. J. *J. Chem. Phys.* **1993**, *98*, 1398.
(42) Michalewicz, M. T.; Brunger, M. J.; McCarthy, I. E.; Norling, V. M. In *CRAY Users Group 1995 Fall Proceedings*; Shaginaw, R., Ed.; Cray Publishing: Alaska, 1995; pp 37−41.
(43) Schmidt, M. W.; Baldridge, K. K.; Boatz, J. A.; Elbert, S. T.; Gordon, M. S.; Jensen, J. J.; Koseki, S.; Matsunaga, N.; Nguyen, K. A.; Su, S.; Windus, T. L.; Dupuis, M.; Montgomery, J. A. *J. Comput. Chem.* **1993**, *14*, 1347.
(44) Knippenberg, S.; Nixon, K. L.; Brunger, M. J.; Maddern, T.; Campbell, L.; Trout, N.; Wang, F.; Newell, W. R.; Deleuze, M. S.; Francois, J.-P.; Winkler, D. A. *J. Chem. Phys.* **2004**, *121*, 10525.
(45) Frost, L.; Weigold, E. *J. Phys. B* **1982** *15*, 2531.
(46) Godbout, N.; Salahub, D. R.; Andzelm, J.; Wimmer, E. *Can. J. Chem.* **1992** *70*, 560.
(47) Dunlap, B. I.; Conolly, J. W. D.; Sabin, J. R. *J. Chem. Phys.* **1979**, *71*, 4993.
(48) Becke, A. D. *J. Chem. Phys.* **1993**, *98*, 5648.
(49) Schirmer, J.; Cederbaum, L. S.; Walter, O. *Phys. Rev. A* **1983**, *28*, 1237.
(50) Schirmer, J.; Angonoa, G. *J. Chem. Phys.* **1989**, *91*, 1754.
(51) Weikert, H.-G.; Meyer, H.-D.; Cederbaum, L. S.; Tarantelli, F. *J. Chem. Phys.* **1996**, *104*, 7122.
(52) Cederbaum, L. S.; Hohlneicher, G.; Peyerimhoff, S. *Chem. Phys. Lett.* **1971**, *11*, 421.
(53) Pickup, B. T.; Goscinski, O. *Mol. Phys.* **1973**, *26*, 1013.
(54) Ohrn, Y.; Born, G. *Adv. Quantum. Chem.* **1981**, *13*, 1.
(55) Deleuze, M. S. *Int. J. Quantum Chem.* **2003**, *93*, 191.
(56) Dunning, T. H. Jr. *J. Chem. Phys.* **1989**, *90*, 1007.
(57) Deleuze, M. S.; Claes, L.; Kryachko, E. S.; Francois, J.-P. *J. Chem. Phys.* **2003**, *119*, 3106.
(58) Liu, B. *Numerical Algorithms in Chemistry, Algebraic Methods, LBL-8158*; Lawrence Berkeley Laboratory: Berkeley, CA.
(59) Tarantelli, F.; Sgamellotti, A.; Cederbaum, L. S.; Schirmer, J. *J. Chem. Phys.* **1987**, *86*, 2201.
(60) Weikert, H.-G.; Meyer, H.-G.; Cederbaum, L. S.; Tarantelli, F. *J. Chem. Phys.* **1996**, *104*, 7122.
(61) Dunning, T. H., Jr. *J. Chem. Phys.* **1971**, *55*, 716.
(62) Martin, J. M.; El-Yazal, J.; Francois, J.-P. *Mol. Phys.* **1995**, *86*, 1437. See also: Koch, W.; Holthausen, M. C. A *A Chemist's Guide to Density Functional Theory*, 2nd ed.; Wiley VCH: Weinheim, Germany, 2001.
(63) Frisch, M. J.; Trucks, G. W.; Schlegel, H. B.; Scuseria, G. E.; Robb, M. A.; Cheeseman, J. R.; Zakrzewski, V. G.; Montgomery, J A.; Stratmann, R. E.; Burant, J. C.; Dapprich, S.; Millam, J. M.; Daniels, A. D.; Kudin, K. N.; Strain, M. C.; Farkas, O.; Tomasi, J.; Barone, V.; Cossi, M.; Cammi, R.; Mennucci, B.; Pomelli, C.; Adamo, C.; Clifford, S.; Ochterski, J.; Petersson, G. A.; Ayala, P. Y.; Cui, Q.; Morokuma, K.; Malick, D. K.; Rabuck, A. D.; Raghavachari, K.; Foresman, J. B.; Cioslowski, J.; Ortiz, J. V.; Stefanov, B. B.; Liu, G.; Liashenko, A.; Piskorz, P.; Komaromi, I.; Gomberts, R.; Martin, R. L.; Fox, D. J.; Keith, T.; Al-Laham, M. A.; Peng, C. Y.; Nanayakkara, A.; Gonsalez, C.; Challacombe, M.; Gill, P. M. W.; Johnson, B. G.; Chen, W.; Wong, M. W.; Andres, J. L.; Head-Gordon, M.; Replogle, E. S.; Pople J. A. *Gaussian98*, revision A.7; Gaussian Inc.: Pittsburgh, PA, 1998.
(64) Cederbaum, L. S.; Domcke, W. *Adv. Chem. Phys.* **1977**, *36*, 205.
(65) Zakrewski, V. G.; von Niessen, W. *J. Comput. Chem.* **1993**, *14*, 13.
(66) Kendall, R. A.; Dunning, T. H., Jr.; Harrison, R. J. *J. Chem. Phys.* **1992**, *96*, 6796.
(67) Deleuze, M. S. *J. Chem. Phys.* **2002**, *116*, 7012.
(68) Deleuze, M. S.; Denis, J. P.; Delhalle, J.; Pickup, B. T. *J. Phys. Chem.* **1993**, *97*, 5115.
(69) Deleuze, M. S.; Delhalle, J.; Pickup, B. T. *Chem. Phys.* **1993**, *175*, 427.
(70) Deleuze, M. S.; Delhalle, J.; Pickup, B. T. *J. Phys. Chem.* **1994**, *98*, 2382.
(71) Deleuze, M. S.; Cederbaum, L. S. *J. Chem. Phys.* **1996**, *105*, 7583.
(72) Golod, A.; Deleuze, M. S.; Cederbaum, L. S. *J. Chem. Phys.* **1999**, *110*, 6014.
(73) Ruhe, A. *Math. Comput.* **1979**, *33*, 680.
(74) Meyer, H.-D.; Pal, S. *J. Chem. Phys.* **1989**, *91*, 6195.
(75) Mackenzie-Ross, H.; Brunger, M. J.; Wang, F.; Adcock, W.; Maddern, T.; Campbell, L.; Newell, W. R.; Weigold, E.; Appelbe, B.; Winkler, D. A. *J. Phys. Chem. A* **2002**, *106*, 9573.
(76) Litvinyuk, I. V.; Zheng, Y.; Brion, C. E. *Chem. Phys.* **2000**, *253*, 41.
(77) Takahashi, M.; Saito, T.; Hiraka, J.; Udagawa, Y. *J. Phys. B* **2003**, *36*, 2539.
(78) Knippenberg, S.; Deleuze, M. S.; Cleij, T. J.; Francois, J.-P.; Cederbaum, L. S.; Eland, J. H. D. *J. Phys. Chem. A* **2005**, *109*, 4267.
(79) Chiang, J. F.; Chiang, R.; Lu, K. C. *J. Mol. Struct.* **1977**, *41*, 67.
(80) Min, J.; Benet-Buchholz, J.; Boese, R. *Chem. Commun.* **1998**, *1*, 2751.
(81) Brunelli, M.; Fitch, A. N.; Jouanneaux, A.; Mora, A. J. *Z. Kristallogr.* **2001**, *216*, 51.
(82) Holthausen, M. C.; Koch, W. *J. Phys. Chem.* **1993**, *97*, 10021.
(83) Yamaguchi, Y.; Frisch, M.; Gaw, J.; Schaefer, H. F., III. *J. Chem. Phys.* **1986**, *84*, 2262.
(84) Jenssen, F. *Introduction to Computational Chemistry*; John Wiley and Sons: Chichester, U.K., 1999.
(85) *Infrared Spectra* in *NIST Chemistry Web Book, NIST Standard Reference Database Number 69*; Linstrom, P. J., Mallard, W. G., Eds.; NIST Mass Spec. Data Centre (Stein, S. E., Director), National Institute of Standards and Technology: Gaithersburg, MD 20899; March 2003 (http://webbook.nist.gov).